Lithos 202–203 (2014) 37–54

Contents lists available at ScienceDirect

Lithos

journal homepage: www.elsevier.com/locate/lithos

Lithosphere thinning beneath west North China Craton: Evidence from geochemical and Sr–Nd–Hf isotope compositions of Jining basalts

Pengyuan Guo [a,*], Yaoling Niu [b,c,d,*], Lei Ye [a], Jinju Liu [a], Pu Sun [a], Huixia Cui [a], Yu Zhang [a], Junping Gao [a], Li Su [d], Jianxin Zhao [e], Yuexing Feng [e]

[a] School of Earth Sciences, Lanzhou University, Lanzhou 730000, China
[b] Institute of Oceanology, Chinese Academy of Sciences, Qingdao 266071, China
[c] Department of Earth Sciences, Durham University, Durham DH1 3LE, UK
[d] School of Earth Science and Mineral Resources, China University of Geosciences, Beijing 100083, China
[e] Radiogenic Isotope Facility, School of Earth Sciences, The University of Queensland, Brisbane QLD 4072, Australia

ARTICLE INFO

Article history:
Received 21 November 2013
Accepted 28 April 2014
Available online 20 May 2014

Keyword:
North China Craton
Cenozoic basalts
Mesozoic basalts
Petrogenesis
Lithosphere thinning
Jining volcanic province

ABSTRACT

This study shows lithosphere evolution history in the west North China Craton (NCC) from the early Cretaceous to Quaternary by studying the major element, trace element and Sr–Nd–Hf isotope compositions in Jining basalts of 119.6–108.6 Ma, 23.5–21.9 Ma and 1.3–0.11 Ma.

The early Cretaceous basalts (119.6–108.6 Ma) display enriched characteristics with high contents of incompatible elements, high $^{87}Sr/^{86}Sr_i$, low $\varepsilon_{Nd}(t)$ and low $\varepsilon_{Hf}(t)$. These basalts resulted from partial melting of ancient metasomatized lithospheric mantle, and we consider the 119.6–108.6 Ma magmatism as indicating lithosphere thinning in the west NCC. Although the Pacific slab seen seismically in the mantle transition zone beneath eastern China is no older than 60 Ma, there exists convincing evidence for the presence of the Paleo-Pacific slab in the transition-zone in the Mesozoic. Thus we propose that the water released from the transition-zone slab hydrated the overlying lithosphere and further converted the base of the lithosphere into asthenosphere. This is the most likely mechanism responsible for the lithosphere thinning in the west NCC and the petrogenesis of the Jining 119.6–108.6 Ma basalts.

The Jining 23.5–21.9 Ma basalts also have high contents of incompatible elements, but they display high $\varepsilon_{Nd}(t)$, high $\varepsilon_{Hf}(t)$ and variably low $^{87}Sr/^{86}Sr_i$. We propose that these Miocene basalts were derived from the asthenosphere with contributions from ancient metasomatized lithospheric mantle during melt ascent. The Jining Quaternary basalts (1.3–0.11 Ma) represent the melt of upwelling asthenosphere with low $^{87}Sr/^{86}Sr_i$, high $\varepsilon_{Nd}(t)$ and high $\varepsilon_{Hf}(t)$. Upwelling and decompression melting of the eastward flowing asthenosphere from beneath western plateaus to beneath eastern hilly plains in the Cenozoic is the most plausible mechanism for the petrogenesis of Jining Cenozoic basalts (both of 23.5–21.9 Ma and 1.3–0.11 Ma), but the Jining 1.3–0.11 Ma basalts must have been produced beneath even thinner lithosphere.

Taken together geophysical studies and our petrological and geochemical studies of all these three episodes of the Jining basalts, we propose that the lithosphere in the west NCC has been thinning since the early Cretaceous and the thinning continues to the present.

1. Introduction

The North China Craton (NCC) is one of the oldest cratons in the world with a history in excess of 3.8 Gyrs (Jahn et al., 1987; Liu et al., 1992). It became a unified craton after the collision between its east and west blocks at 1.8 Ga and remained stable until the late Paleozoic (Zhao et al., 2001). Some authors (e.g., Menzies and Xu, 1998; Ye et al., 1987) consider the NCC to consist of two different tectonic domains separated by the North–South trending Daxinganling–Taihangshan gravity lineament (Fig. 1a). This North–South gravity lineament (NSGL) marks a sharp elevation contrast in continental China between the high plateaus to the west and hilly plains to the east. The lineament is better termed as the Great Gradient Line (GGL; Niu, 2005) because it not only is a gravity lineament, but also displays steep gradients in, for example, elevation, topography, crustal thickness, lithosphere thickness, heat flow and upper mantle seismic velocity structures. On the other hand, recent studies (e.g., Zhao et al., 2001) prefer to divide the North China Craton into East Block, West Block and the intervening Trans-North China Orogen (TNCO; Fig. 1a) on the basis of age, lithological assemblage, geochemistry and metamorphic

* Corresponding authors at: School of Earth Sciences, Lanzhou University, 222 Tianshui Road, Lanzhou, Gansu, China.
E-mail addresses: guopy12@lzu.edu.cn (P. Guo), yaoling.niu@foxmail.com (Y. Niu).

http://dx.doi.org/10.1016/j.lithos.2014.04.024
0024-4937/

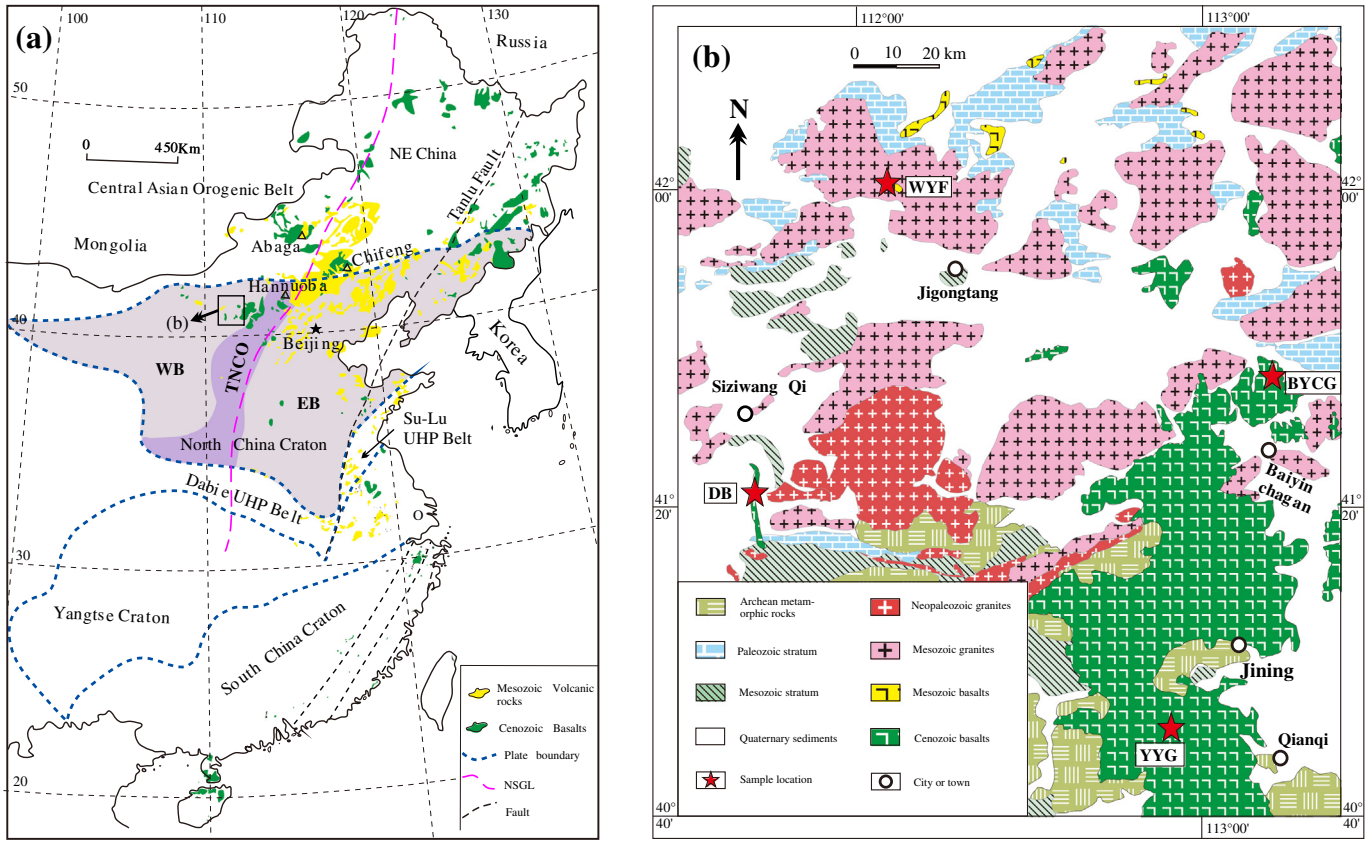

Fig. 1. (a) Sketch map of major tectonic divisions of China. WB, TNCO and EB denote three divisions of the North China Craton into the Western Block, Trans-North China Orogen and Eastern Block, respectively (Zhao et al., 2001). NSGL indicates the North–South Gravity Lineament. (b) The distribution and sample locations of Jining basalts. Samples from location WYF are dated at 119.6–108.6 Ma (Zhang et al., 2005), from location DB dated at 21.9 Ma (Chen et al., 2004), from location YYG dated at 23.5–23.3 Ma (Zhao et al., 2013), and from location BYCG dated at 1.3–0.11 Ma (Ho et al., 2008).

history of basement rocks (e.g., P–T–t paths). The East Block consists predominantly of Archean tonalitic–trondhjemitic–granodiotitic (TTG) batholiths. The late Archean lithological assemblage, structural style and metamorphic history in the West Block are similar to those of the East Block. The TNCO is composed of late Archean to Paleoproterozoic TTG gneisses and granitoids, interleaved with abundant sedimentary and volcanic rocks, which underwent compressional deformation with peak high-pressure metamorphism at the late Paleoproterozoic (2.0–1.8 Ga; Zhao et al., 2001).

Unlike other stable cratons (e.g., Kaapvaal Craton and Zimbabwe Craton in South Africa, Slave Craton in North America and Siberia Craton; Carlson et al., 2005), the North China Craton experienced widespread tectonothermal activity since the late Mesozoic (Chen, 1960; Deng, 1988; Menzies and Xu, 1998; Wong, 1929), which changed the old, cold, thick and metasomatically-enriched fertile "cratonic" mantle lithosphere into a young, warm, thin and depleted mantle lithosphere (Griffin et al., 1998; Menzies et al., 1993; Xu, 2001). This tectonothermal activity was accompanied by large scale calc-alkaline and alkaline volcanisms, development of large sedimentary basins, high surface heat flow and a change in the geochemistry of mantle xenoliths carried by Mesozoic and Cenozoic basalts (e.g., Fan et al., 2000; Gao et al., 2002; Griffin et al., 1998; Ren et al., 2002; Xu, 2001). Mantle plumes have been proposed as a mechanism causing the Mesozoic lithosphere thinning and volcanism through to the Cenozoic in eastern China (Deng et al., 1998, 2004), but the observation that the "cold" subducted Paleo-Pacific slab lies in the mantle transition-zone (between 410 and 660 km seismic discontinuities) beneath eastern China (Kárason and Van der Hilst, 2000; Zhao, 2009) argues against the presence and working of hot mantle plumes beneath eastern China (Niu, 2005). Other interpretations on the lithosphere thinning or "destruction" of the NCC include: (1) lithosphere delamination (e.g., Gao et al., 2004, 2009; Xu et al., 2006); (2) thermal and chemical erosion (e.g., Griffin et al., 1998; Menzies et al., 1993; Xu, 2001); and (3) basal hydration weakening that converts the base of the lithosphere into asthenosphere in terms of physical properties (Niu, 2005).

It should be noted, however, that all the above interpretations on the NCC lithosphere thinning have been based on studies of Mesozoic and Cenozoic volcanic rocks and their xenoliths in the East North China Block (i.e., EB in Fig. 1a; e.g., Deng et al., 1998, 2004; Gao et al., 2004; Wu et al., 2003; Xu, 2001; Xu et al., 2006; Zhang et al., 2002) and Trans-North China Orogen (i.e., TNCO in Fig. 1a; e.g., Tang et al., 2006; Xu et al., 2005). Few Mesozoic and Cenozoic volcanic rocks from the West North China Block have been reported until Chen et al. (2004) mostly because of their rarity. Chen et al. (2004) first described mantle xenoliths hosted in the Miocene basalts in Siziwang Qi, Inner Mongolia (Fig. 1b), and there have been recent petrological and geochemical studies on these basalts and their hosted crustal and mantle xenoliths (He et al., 2009; Ho et al., 2011; Jing et al., 2010; Li et al., 2006; Yang et al., 2009; Zhang and Han, 2006; Zhang et al., 2005, 2012a, 2012b).

In this paper, we present major element, trace element and Sr–Nd–Hf isotope data on basalts of the early Cretaceous (119.6–108.6 Ma; Zhang et al., 2005), Miocene (23.5–21.9 Ma; Chen et al., 2004; Zhao et al., 2013) and Quaternary (1.3–0.11 Ma; Ho et al., 2011) in Jining area (in the West North China Block) with the aim of understanding their source compositional changes through time, which may reflect lithosphere evolution of the region, and may thus offer new perspectives on the NCC destruction on a greater spatial scale than previously thought.

2. Geological setting and samples

Jining, in central Inner Mongolia, is located near the northern margin of the west NCC (Zhao et al., 2001). To the north is the Central Asian Orogenic Belt, which is the result of closure of the Paleo-Asian Ocean in the late Jurassic (Yin and Nie, 1996). Alkaline volcanism (spatially scattered) occurred in the Jining area during the early Cretaceous (Li et al., 2006; Zhang et al., 2005), and Zhang et al. (2005) suggested that these alkaline basalts are shoshonites. The Cenozoic saw a large scale of volcanic activities (>~8000 km^2) in this region, forming the Jining Cenozoic volcanic province (Ho et al., 2011; Zhang and Han, 2006; Zhang et al., 2012b), which is the westernmost volcanic province in the NCC. This volcanic province could be genetically related to other Cenozoic volcanic provinces nearby such as Hannuoba (Zhi et al., 1990), Chifeng (Han et al., 1999), and Abaga (Ho et al., 2008). The Jining Cenozoic basaltic volcanism spanned a long period from the late Oligocene to the Quaternary (~33–~0.1 Ma) as evidenced by K–Ar dating, stratigraphy and paleontology (Chen et al., 2004; Ho et al., 2011; Luo and Chen, 1990; Zhang and Han, 2006; Zhao et al., 2013). Zhang et al. (2012b) considered that the eruption mostly occurred in the Miocene.

In this study, we discuss the results of our study on Jining basalt samples collected from four locations (Fig. 1b), ranging in age from early Cretaceous (119.6–108.6 Ma; Zhang et al., 2005) to Miocene (23.5–21.9 Ma; Chen et al., 2004; Zhao et al., 2013) and to Quaternary (1.3–0.11 Ma; Ho et al., 2011).

2.1. Early Cretaceous basalts of 119.6–108.6 Ma

The 119.6–108.6 Ma basalts are scattered in the Siziwang Qi area (Fig. 1b; 112°00′–113°00′E, 42°00′–42°15′N) with highly restricted outcrops because of the vast grassland. Zhang et al. (2005) first reported these basalts and gave a K–Ar age of 119.6–108.6 Ma. The samples (named WYF) in this study were collected in an open pit (112°01′13.0″E; 41°59′16.3″N), ~80 km northeast of Siziwang Qi (Fig. 1b). These basalts are massive flows, containing abundant granulite xenoliths (He et al., 2009). The samples are porphyric with <5% phenocrysts, mostly plagioclase (~0.5–~1.0 mm in size) and minor olivine and Fe–Ti oxides (Fig. 2a, b). The groundmass consists of quench plagioclase, olivine, clinopyroxene and Fe–Ti oxides.

2.2. Miocene basalts of 23.5–21.9 Ma

Our 23.5–21.9 Ma samples were collected from Dongba and Youyinggou (see Fig. 1b), the westernmost Cenozoic basalt outcrops in the NCC. The Dongba (named DB) basalts crop out ~20 km south of Siziwang Qi (Fig. 1b; 111°43′46.5″E; 41°22′45.6″N). Chen et al. (2004) reported a whole-rock K–Ar age of 21.9 Ma for the Dongba basalts. These basalts are fresh and porphyritic with <10% phenocrysts of olivine (0.2–0.5 mm in size). The groundmass consists of olivine + clinopyroxene + plagioclase + Fe–Ti oxides (Fig. 2c). These basalts also contain abundant mantle (spinel lherzolite) and crustal (granulite) xenoliths (Jing et al., 2010).

Youyinggou basalts (named YYG) were sampled from ~30 km southwest of Jining City (112°52′35.9″E, 40°50′17.8″E; Fig. 1b). Zhao et al. (2013) recently gave a whole-rock K–Ar age of 23.50–23.35 Ma for these basalts. Youyinggou basalts are fresh and porphyritic, with <5% phenocrysts of olivine (0.2–0.5 mm). The groundmass consists of olivine + clinopyroxene + Fe–Ti oxides (Fig. 2d). Mantle xenoliths (spinel lherzolite and minor phlogopite-bearing spinel lherzolite) are common in these basalts (Zhang et al., 2012a; Zhao et al., 2013).

2.3. Quaternary basalts of 1.3–0.11 Ma

The Baiyinchagan volcano group, ~80 km north of Jining, including ~30 volcanic cones, covers an area of ~280 km^2 (Bai et al., 2008). The volcanic rocks are mainly lava flows with pyroclastics and scoria. Ho et al. (2011) reported the bulk-rock K–Ar age of 1.3–0.11 Ma for these basalts. The massive flow sample (BYCGI-03) was collected along the roadside (113°06′12.1″E, 41°34′51.1″N). This sample is porphyritic with ~25% phenocrysts (Fig. 2e), mostly well oriented plagioclase (0.5–2.0 mm in size) with minor clinopyroxene (0.5–1.0 mm in size). Our samples collected from two volcanic cones north of Baiyinchagan (named BYCGII and BYCGIII) are very fresh vesicular basalts (vesicular >60%) with few phenocrysts (see Fig. 2f).

3. Sample preparation and analytical procedures

We chose the freshest samples for geochemical analysis. Weathered surfaces, pen marks and saw marks were ground off and thoroughly cleaned. The samples were then crushed into chips of ~0.5 cm to select fresh matrix material so as to obtain basaltic melt compositions. The matrix material was then ultrasonically-cleaned with Milli-Q water and dried before powdered using an agate mill under a clean environment.

Bulk-rock major element oxides were analyzed using a Leeman Prodigy inductively coupled plasma-optical emission spectrometer (ICP-OES) at China University of Geosciences, Beijing (CUGB). Precisions (1σ) for most elements based on rock standards GSR-1, GSR-3 (National Geological Standard Reference Materials of China) and AGV-2 (US Geological Survey) are better than 1.0% with the exception of TiO_2 (<1.5%) and P_2O_5 (1.0–1.5%). Loss on ignition (LOI) was determined by placing 500 mg of samples in the muffle furnace at 1000 °C for several hours before cooled in a desiccator and reweighed.

Whole-rock trace element analysis was done using an Agilent-7500a inductively coupled plasma mass spectrometer (ICP-MS) at CUGB. Thirty five milligram powder of each sample was dissolved with acid mix (1:1) of distilled HF and HNO_3 in a high-pressure jacket equipped Teflon beaker in an oven for 48 h to ensure complete digestion/dissolution. This procedure was repeated using larger amounts of acids for a further 24 h. After digestion, the sample was evaporated to incipient dryness, refluxed with 6 N HNO_3, and heated again to incipient dryness. The sample was then dissolved in 2 ml 3 N HNO_3 and diluted with Milli-Q water (18 MΩ) to a final dilution factor of 2000. Rock standards GSR-1, GSR-3 and AGV-2 were used to monitor the analytical accuracy and precision (see Appendix 1). Analytical accuracy, as indicated by relative difference between measured and recommended values, is better than 5% for most elements, and 5–15% for Gd, and Ta.

For samples DB-01, DB-07, WYF-10, WYF-19, BYCGI-03, BYCGII-02, BYCGIII-05 and BYCGIII-12, the bulk-rock Sr, Nd and Hf elemental separation was done in the Institute of Geology and Geophysics (Beijing), Chinese Academy of Sciences (IGG-CAS). Analytical details for sample digestion and column separation procedures are described in Yang et al. (2010). Strontium isotope ratios were determined using Thermal Ionization Mass Spectrometer (TIMS) in Tianjin Institute of Geology and Mineral Resources. The measured $^{87}Sr/^{86}Sr$ ratios were corrected for mass-fractionation using $^{86}Sr/^{88}Sr = 0.1194$. During our sample analysis, the measured values for NBS-987 Sr standard is $^{87}Sr/^{86}Sr = 0.710250 \pm 5$ (n = 4, 2SD). Neodymium isotope analysis was done using a Multi-Collector Inductively Coupled Plasma Mass Spectrometer (MC ICP-MS) at China University of Geosciences, Wuhan (CUGW). The measured $^{143}Nd/^{144}Nd$ ratios were corrected for mass fractionation to $^{146}Nd/^{144}Nd = 0.7219$ and the analysis of standard JNdi-1 Nd gave $^{143}Nd/^{144}Nd = 0.512101 \pm 4$ (n = 7, 2SD). Hafnium isotopic ratios were determined using MC ICP-MS in the IGG-CAS (Yang et al., 2010). The $^{176}Hf/^{177}Hf$ ratios were normalized to $^{179}Hf/^{177}Hf = 0.7325$ using the exponential law for mass-bias correction (Wu et al., 2006). During our sample analysis, an Alfa Hf standard was measured 11 times and gave an average $^{176}Hf/^{177}Hf$ value of 0.282169 ± 6 (n = 11, 2SD). The values of USGS reference materials BCR-2 and BHVO-2 run with our samples are given in Appendix 2.

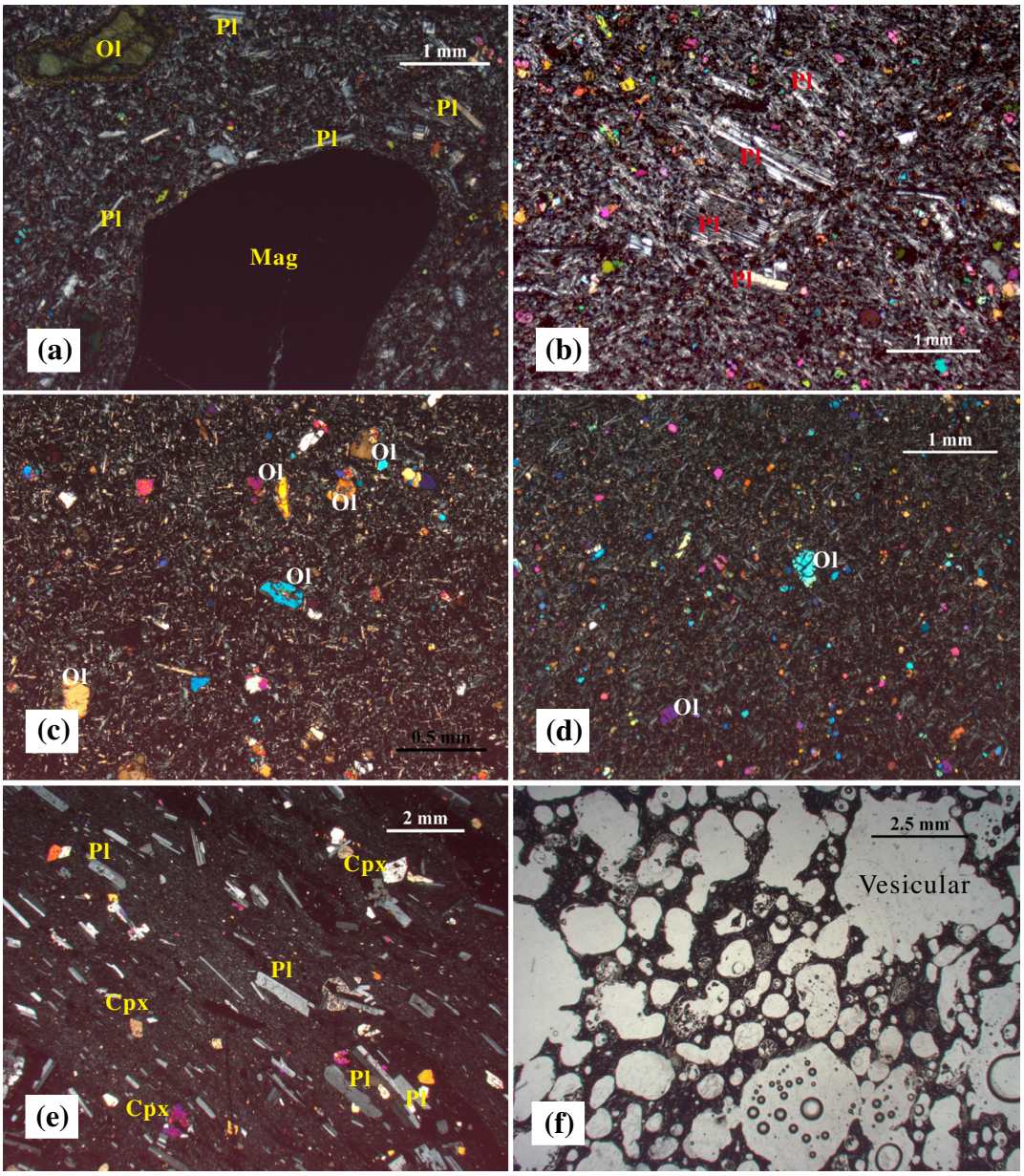

Fig. 2. Photomicrographs of representative Jining basalt samples. (a) Sample WYF-05, XPL, magnetite megacryst and olivine phenocryst; (b) sample WYF-19, XPL, plagioclase phenocrysts and the matrix composed of plagioclase, olivine and magnetite; (c) sample DB-02, XPL, olivine phenocrysts and the matrix composed of plagioclase, olivine and magnetite; (d) sample YYG-08, XPL, olivine phenocrysts and the matrix composed of plagioclase, olivine and magnetite; (e) sample BYCGI-03, XPL, ~25% plagioclase phenocrysts and minor clinopyroxene phenocrysts; and (f) sample BYCGIII-01, PPL, 60% vesicles and 40% matrix make up the Jining Quaternary vesicular basalts.

For samples DB-02, DB-03, WYF-05, WYF-07, and WYF-09, the bulk-rock Sr–Nd–Hf isotopic compositions were analyzed in the Radiogenic Isotope Facility at the University of Queensland, Australia. Analytical details for sample digestion and Sr, Nd and Hf elemental column separation procedures are described in Feng et al. (in preparation). In brief, about 100 mg of basaltic rock powder samples were dissolved in the mixture of double-distilled concentrate HNO_3 and HF, and dried down on a hot plate at 80 °C. After converting any fluoride to nitrate, the dried residue was dissolved with 3 ml 2 N HNO_3 and 1.5 ml was loaded onto a stack of Sr-spec, Thru-spec and LN-spec resin columns to separate Sr, Nd, and Hf from matrix, using a streamlined procedure modified after Mikova and Denkova (2007) and Yang et al. (2010). Procedural blanks are ca. 65, 60, and 16 pg for Sr, Nd and Hf, respectively. The measurement of $^{87}Sr/^{86}Sr$, $^{143}Nd/^{144}Nd$ and $^{176}Hf/^{177}Hf$ ratios was conducted in static mode on a Nu Plasma HR MC-ICP-MS using a modified CETAC ASX-110FR auto-sampler and a DSN-100 dissolvation nebulizing system. The measured $^{87}Sr/^{86}Sr$, $^{143}Nd/^{144}Nd$ and $^{176}Hf/^{177}Hf$ ratios were corrected for mass fractionation using the exponential law by normalizing to $^{86}Sr/^{88}Sr = 0.1194$, $^{146}Nd/^{144}Nd = 0.7219$ and $^{179}Hf/^{177}Hf = 0.7325$, respectively. Instrument drift was monitored and calibrated with standards. During our sample analysis, the measured average value for NBS-987 Sr standard is $^{87}Sr/^{86}Sr = 0.710248 \pm 9$ (n = 26, 2SD), identical to our previous long-term average (0.710249 ± 28) measured using TIMS. An in-house Nd standard, Ames Nd Metal, was used as an Nd isotope drift monitor. In the cross-calibration of the Nd Metal against the international standard JNdi-1, 17 measurements of the Nd Metal yielded an average $^{143}Nd/^{144}Nd$ of 0.511966 ± 16 (n = 20, 2SD), corresponding to an average JNdi-1 $^{143}Nd/^{144}Nd$ of 0.512113 ± 9 (n = 20, 2SD), which is within error of the consensus value (0.512115 ± 7). During our analysis, 39 measurements of Nd Metal yielded a mean $^{143}Nd/^{144}Nd$ of 0.511967 ± 8 (n = 39, 2SD). During measurement of $^{176}Hf/^{177}Hf$ ratios, 10 ppm Hf ICP solution

Table 1
Bulk rock major (wt.%) and trace (ppm) element analysis for Jining basalts.

Age	119.6–108.6 Ma (Zhang et al., 2005)					23.5–23.4 Ma (Zhao et al., 2013)					
Sample no.	WYF-05	WYF-07	WYF-09	WYF-10	WYF-19	YYG-01	YYG-03	YYG-08	YYG-10	YYG-11	YYG-16
SiO_2	49.4	49.9	51.2	49.9	51.7	48.9	48.8	47.6	47.7	48.7	48.0
TiO_2	2.60	2.56	2.47	2.47	2.44	1.80	1.80	1.92	1.87	1.70	1.85
Al_2O_3	15.4	15.1	14.8	15.1	14.9	14.6	14.9	14.9	15.1	14.2	14.8
$^{T}Fe_2O_3$	11.0	10.8	10.6	10.5	10.5	11.7	11.7	12.2	12.0	11.4	12.0
MnO	0.15	0.15	0.14	0.14	0.14	0.15	0.15	0.16	0.16	0.16	0.16
MgO	5.63	5.64	5.48	5.30	5.23	5.38	5.18	6.18	5.53	6.47	5.58
CaO	6.71	6.75	6.48	6.93	6.21	6.70	6.51	7.24	6.79	7.26	6.83
Na_2O	3.94	3.87	3.79	3.49	4.07	4.90	5.08	4.24	4.85	4.78	4.97
K_2O	2.58	2.65	2.48	2.59	2.47	2.79	2.90	2.46	2.78	2.14	2.68
P_2O_5	0.63	0.61	0.59	0.64	0.60	0.84	0.84	0.75	0.88	0.73	0.84
LOI	1.29	1.31	1.23	2.09	1.13	1.68	1.55	1.75	1.66	1.90	1.73
$Mg^{\#a}$	0.53	0.53	0.53	0.53	0.52	0.50	0.49	0.53	0.50	0.56	0.51
Sc	16.2	16.5	16.0	15.8	15.6	10.3	11.1	13.0	10.3	13.0	10.3
V	205	215	203	201	199	107	115	129	108	132	108
Cr	78.0	83.4	79.1	84.6	78.1	87.0	82.1	103	83.8	145	81.4
Ni	48.3	49.1	47.6	49.3	46.2	85.5	87.9	104	87.2	110	87.3
Rb	56.2	61.0	54.6	57.8	48.5	28.3	31.3	25.4	29.5	29.9	28.5
Sr	811	903	852	1375	795	1024	1156	888	991	932	1019
Y	21.6	21.8	21.2	21.5	21.6	18.6	20.1	19.2	18.7	17.9	18.5
Zr	230	233	224	231	230	386	418	337	389	348	380
Nb	70.7	71.1	69.0	70.8	70.6	95.8	105	82.0	96.4	84.8	94.8
Ba	889	892	875	877	888	305	336	909	310	275	304
La	31.6	31.5	30.6	31.6	31.4	54.2	58.9	46.1	55.0	48.1	53.6
Ce	65.4	66.1	63.6	65.6	64.7	93.6	103	86.9	95.2	90.0	92.6
Pr	8.68	8.95	8.44	8.67	8.54	12.4	13.4	10.8	12.6	11.1	12.3
Nd	32.7	33.7	31.9	32.7	32.1	45.0	48.5	39.5	45.6	40.4	44.6
Sm	6.29	6.32	6.19	6.27	6.21	8.83	9.49	7.99	8.90	8.07	8.79
Eu	2.09	2.08	2.06	2.08	2.07	2.77	2.96	2.59	2.80	2.51	2.75
Gd	5.52	6.02	5.39	5.53	5.45	7.29	7.89	6.82	7.40	6.77	7.25
Tb	0.80	0.81	0.79	0.80	0.80	1.00	1.08	0.96	1.02	0.94	1.00
Dy	4.02	4.01	3.92	3.96	3.94	4.34	4.66	4.31	4.38	4.10	4.31
Ho	0.81	0.81	0.79	0.80	0.81	0.73	0.78	0.76	0.74	0.70	0.73
Er	1.96	1.97	1.93	1.96	1.97	1.49	1.59	1.62	1.50	1.44	1.50
Tm	0.29	0.29	0.29	0.29	0.29	0.18	0.20	0.21	0.19	0.18	0.19
Yb	1.59	1.60	1.57	1.60	1.60	0.90	0.97	1.07	0.91	0.90	0.90
Lu	0.23	0.23	0.23	0.23	0.23	0.12	0.12	0.14	0.12	0.12	0.12
Hf	5.28	5.33	5.19	5.30	5.32	8.86	9.66	7.91	9.10	8.04	8.76
Ta	4.34	4.37	4.27	4.40	4.40	5.69	6.17	4.86	5.72	4.97	5.59
Pb	3.67	3.69	3.40	5.99	3.78	3.63	6.07	3.80	3.93	3.28	3.86
Th	2.53	2.52	2.42	2.58	2.61	5.29	5.82	4.72	5.43	4.65	5.24
U	0.65	0.67	0.63	0.69	0.70	1.62	1.81	1.47	1.70	1.42	1.63

Age	23.5–23.4 Ma (Zhao et al., 2013)		21.9 Ma (Chen et al., 2004)					1.3–0.11 Ma (Ho et al., 2011)			
Sample no.	YYG-17	YYG-18	DB-01	DB-02	DB-03	DB-07	BY I-03	BY II-02	BYIII-05	BYIII-10	BYIII-12
SiO_2	45.8	47.3	43.5	43.3	44.3	47.8	48.3	49.1	48.9	46.6	47.5
TiO_2	2.08	2.50	2.36	2.39	2.35	2.64	2.23	2.27	2.51	2.58	2.56
Al_2O_3	14.5	13.8	14.0	13.7	13.5	13.7	14.4	14.6	15.3	15.7	15.9
$^{T}Fe_2O_3$	13.1	12.0	12.4	12.9	12.6	12.9	11.8	11.9	11.4	11.7	11.6
MnO	0.17	0.15	0.16	0.17	0.17	0.16	0.16	0.15	0.15	0.15	0.15
MgO	7.29	7.64	7.66	8.28	7.88	6.10	7.16	5.69	4.14	4.25	4.22
CaO	7.87	7.30	7.68	7.79	7.73	6.97	8.50	8.49	7.65	7.73	7.98
Na_2O	4.12	4.45	6.20	5.72	5.61	4.46	4.02	4.36	4.94	5.06	5.21
K_2O	2.35	1.36	1.97	2.21	2.12	1.41	1.04	1.96	2.89	2.97	2.97
P_2O_5	0.58	1.01	1.42	1.47	1.44	1.01	0.56	0.64	0.91	0.95	0.96
LOI	1.49	1.91	1.85	1.49	1.71	1.96	1.25	0.14	0.30	1.52	0.23
$Mg^{\#}$	0.55	0.58	0.58	0.59	0.58	0.51	0.57	0.51	0.44	0.44	0.44
Sc	13.7	12.9	8.95	9.02	9.56	9.95	20.3	16.3	10.6	10.6	10.4
V	145	135	118	122	126	146	192	191	174	185	169
Cr	113	147	124	115	127	110	160	126	17.4	14.7	16.5
Ni	113	126	129	125	114	94.7	128	55.3	24.2	22.0	20.0
Rb	25.2	29.1	26.9	31.5	36.4	42.7	22.0	27.9	36.9	36.7	36.0
Sr	714	1149	1365	1535	1554	1099	645	686	893	890	872
Y	16.2	22.8	23.1	23.5	24.1	21.6	22.5	19.7	19.7	19.4	19.0
Zr	293	319	359	356	364	370	211	214	262	262	254
Nb	65.4	93.1	135	134	138	114	54.4	59.7	89.2	89.5	86.8
Ba	244	458	358	372	375	568	404	414	534	521	517
La	34.2	42.9	62.1	63.0	64.8	51.0	24.3	28.8	38.4	38.2	37.2
Ce	66.3	85.8	107	110	113	93.2	48.3	54.7	71.2	70.9	69.1
Pr	7.92	11.5	14.3	14.6	15.0	12.8	6.29	6.98	8.83	8.75	8.55
Nd	32.3	44.6	53.2	54.5	55.7	48.4	24.0	26.5	32.7	32.5	31.6
Sm	6.81	9.23	10.9	11.1	11.4	10.1	5.26	5.77	6.74	6.64	6.49

(continued on next page)

Table 1 (*continued*)

Age	23.5–23.4 Ma (Zhao et al., 2013)		21.9 Ma (Chen et al., 2004)					1.3–0.11 Ma (Ho et al., 2011)			
Sample no.	YYG-17	YYG-18	DB-01	DB-02	DB-03	DB-07	BY I-03	BY II-02	BYIII-05	BYIII-10	BYIII-12
Eu	2.21	2.95	3.47	3.53	3.62	3.19	1.75	1.90	2.20	2.16	2.10
Gd	6.01	8.01	9.22	9.46	9.68	8.57	5.07	5.44	6.04	5.90	5.82
Tb	0.81	1.11	1.25	1.28	1.31	1.16	0.80	0.81	0.87	0.85	0.84
Dy	4.07	5.02	5.41	5.54	5.65	5.01	4.16	3.91	4.06	3.96	3.89
Ho	0.67	0.89	0.90	0.92	0.94	0.85	0.85	0.74	0.75	0.73	0.72
Er	1.64	1.92	1.80	1.83	1.84	1.67	2.10	1.67	1.64	1.61	1.58
Tm	0.20	0.25	0.21	0.22	0.21	0.20	0.31	0.23	0.22	0.22	0.21
Yb	1.16	1.25	0.96	0.99	0.99	0.95	1.71	1.19	1.12	1.10	1.07
Lu	0.16	0.17	0.12	0.12	0.12	0.12	0.25	0.16	0.15	0.15	0.14
Hf	6.91	7.61	8.14	8.08	8.11	8.76	4.76	5.01	5.81	5.75	5.61
Ta	3.92	5.45	7.77	8.10	8.19	7.33	3.32	3.62	5.38	5.36	5.22
Pb	3.01	31.4	3.56	3.56	3.62	4.31	2.16	2.84	3.52	3.18	4.22
Th	3.23	4.40	6.43	6.18	6.25	5.31	2.15	2.80	4.12	4.07	4.00
U	1.02	1.23	2.13	1.98	2.04	1.34	0.69	0.76	1.16	1.15	1.12

[a] Mg# = molar Mg / (Mg + Fe^{2+}).

from Choice Analytical was used as the instrument drift monitor. This in-house standard was cross-calibrated against JMC-475 Hf international standard through parallel bracketing measurements. Its repeated measurements yield a mean $^{176}Hf/^{177}Hf$ of 0.282145 ± 6 (n = 16, 2SD), corresponding to a mean value of 0.282160 ± 6 (n = 16, 2SD) for JMS-475 standard. During our sample analysis, the in-house Hf standard monitor was measured between every 5 samples and 37 repeated measurements gave an average $^{176}Hf/^{177}Hf$ value of 0.282133 ± 3 (n = 37, 2SD), which was used to correct instrumental drift on measured sample ratios relative to JMS-475 Hf standard. The values of USGS reference materials BCR-2 and BHVO-2 run with our samples are given in Appendix 2, which are consistent with the reported reference values (GeoREM, http://georem.mpch-mainz.gwdg.de/).

4. Results

Table 1 gives the major and trace element data and Table 2 presents the Sr–Nd–Hf isotope data. Initial Sr–Nd–Hf isotopic ratios were calculated using the emplacement ages of 119.6 Ma and 23.5 Ma for Jining basalts, respectively. We did not calculate initial isotopic ratios for the young Quaternary Jining basalts.

4.1. Major element data

All the five Jining 119.6–108.6 Ma samples display a narrow compositional range and high total alkalis ($Na_2O + K_2O$ = 6.08–6.55 wt.%), and can be termed basaltic trachyandesite (see Fig. 3). They are hypersthene or nepheline normative (Fig. 4) and can be further classified as olivine tholeiites and alkali olivine basalts using the Ne–Ol–Di–Hy–Qz tetrahedron. While the 119.6–108.6 Ma basalts show small compositional variation, the correlated trends are apparent in MgO-variation diagrams of SiO_2, TiO_2 and $^{T}Fe_2O_3$ (Fig. 5).

The Jining 23.5–21.9 Ma basalts display lower SiO_2 and a slightly higher total alkalis ($K_2O + Na_2O$ = 5.80–8.17 wt.%). They are nepheline-normative and can be termed alkali olivine basalts in general (Fig. 4). These Miocene basalts have a larger range of MgO and form good compositional trends in MgO-variation diagrams (Fig. 5). For instance, TiO_2, $^{T}Fe_2O_3$, CaO/Al_2O_3, Cr and Ni correlate positively with MgO while SiO_2 and Al_2O_3 increase with decreasing MgO. Note that the decreasing TiO_2 with decreasing MgO is inconsistent with the trend being a low-pressure liquid line of descent.

The Jining Quaternary basalts (1.3–0.11 Ma) have low SiO_2 (Fig. 3) and a relatively large range of MgO (Fig. 5). They have high TiO_2 (all >2.20 wt.%) and their $K_2O + Na_2O$ ranges from 5.06 wt.% to 8.18 wt.%. Like those 23.5–21.9 Ma basalts, the Quaternary samples are all nepheline-normative (Fig. 4). Despite the limited number of samples, they form compositional trends similar to those defined by the 23.5–21.9 Ma basalts except for TiO_2, which displays an inverse TiO_2–MgO trend qualitatively consistent with a low-pressure liquid line of descent (Fig. 5).

4.2. Trace element data

In chondrite-normalized rear earth element (REE) diagram (Fig. 6a), the 119.6–108.6 Ma basalts show uniform compositions, enriched in light rare earth elements (LREEs) and depleted in heavy rare earth elements (HREEs) with $[La/Yb]_N$ = 14.0–14.3, resembling average composition of present-day ocean island basalts (OIB). In primitive mantle normalized multi-trace element spidergram (Fig. 6b), these samples exhibit OIB-like trace element patterns with outstanding Nb and Ta positive anomalies relative to Th and U. Note that sample WYF-10 shows higher Pb and Sr, and we consider this may be due to post-magmatic process (also see below).

In comparison, the 23.5–21.9 Ma basalts are more enriched in LREEs with significantly greater $[La/Yb]_N$ = 21.1–47.0. In primitive mantle normalized multi-trace element spidergram (Fig. 6d), these basalts display similar elemental patterns to those defined by the 119.6–108.6 Ma basalts, but show even greater Nb and Ta enrichments relatively to Ba, Rb and LREEs.

The Quaternary basalts also have OIB-like REE patterns with $[La/Yb]_N$ = 10.2–25.0 (Fig. 6e). In primitive mantle normalized multi-trace element spidergram (Fig. 6f), these Quaternary basalts display similar characteristics when compared with the 119.6–108.6 Ma basalts, i.e., conspicuous positive Nb and Ta anomalies with essentially no Ti anomaly (see Fig. 6f).

In general, the abundances of Rb, Ba, Nb, Ta, U, Sr, La, Pb, Zr and Nd are well correlated with Th in Jining basalts of 23.5–21.9 Ma and 1.3–0.11 Ma. However, a small number of 23.5–21.9 Ma samples show anomalously high Rb and Ba (Fig. 7a, b). In comparison, the 119.6–108.6 Ma basalts display very limited variation of trace elements (Fig. 7), but show significantly higher Rb and Ba than the Jining Cenozoic basalts (both of 23.5–21.9 Ma and 1.3–0.11 Ma; Fig. 7a, b).

4.3. Sr–Nd–Hf isotopes

The 119.6–108.6 Ma basalts show enriched isotopic compositions with a large range of elevated $^{87}Sr/^{86}Sr_i$ (0.706002–0.708542), restricted $^{143}Nd/^{144}Nd_i$ (0.512319–0.512338; corresponding to $\varepsilon_{Nd}(t)$ = ~−4.16), and restricted $^{176}Hf/^{177}Hf_i$ (0.282725–0.282739; corresponding to $\varepsilon_{Hf}(t)$ = ~−0.07). In Sr–Nd isotope space (Fig. 8a), the five

Table 2
Bulk rock Sr–Nd–Hf isotope analysis for Jining basalts.

Sample name	Age	$^{87}Rb/^{86}Sr$[a]	$^{87}Sr/^{86}Sr$ (2σ)	$^{87}Sr/^{86}Sr_i$[b]	$^{147}Sm/^{144}Nd$[a]	$^{143}Nd/^{144}Nd$ (2σ)	$^{143}Nd/^{144}Nd_i$[b]	$^{176}Lu/^{177}Hf$[a]	$^{176}Hf/^{177}Hf$ (2σ)	$^{176}Hf/^{177}Hf_i$[b]	$\varepsilon_{Nd}(t)$[c]	$\varepsilon_{Hf}(t)$[c]
WYF-05	119.6–108.6 Ma	0.200711	0.706316 ± 13	0.706002	0.115822	0.512422 ± 6	0.512324	0.006231	0.282775 ± 6	0.282735	−4.22	0.11
WYF-07	(Zhang et al., 2005)	0.195825	0.707094 ± 11	0.706788	0.113055	0.512414 ± 6	0.512319	0.006221	0.282779 ± 7	0.282739	−4.36	0.25
WYF-09		0.185654	0.706587 ± 11	0.706296	0.116803	0.512418 ± 5	0.512320	0.006227	0.282778 ± 7	0.282739	−4.28	0.23
WYF-10		0.121772	0.708732 ± 8	0.708542	0.115276	0.512435 ± 1	0.512338	0.006138	0.282764 ± 14	0.282725	−3.96	−0.27
WYF-19		0.176771	0.706769 ± 4	0.706492	0.116378	0.512433 ± 2	0.512335	0.006206	0.282773 ± 17	0.282733	−3.99	0.03
YYG-03	23.5–23.4 Ma	0.078393	0.704346 ± 6	0.704320	0.117811	0.512893 ± 2	0.512875	0.001829	0.283041 ± 11	0.283038	4.97	9.50
YYG-17	(Zhao et al., 2013)	0.102200	0.703818 ± 6	0.703784	0.127107	0.512849 ± 1	0.512829	0.003298	0.28301 ± 12	0.283006	4.11	8.41
DB-01	21.9 Ma	0.057006	0.703620 ± 4	0.703602	0.123551	0.512967 ± 1	0.512949	0.002035	0.283081 ± 10	0.283079	6.41	10.94
DB-02	(Chen et al., 2004)	0.059482	0.704327 ± 11	0.704308	0.122613	0.512957 ± 5	0.512940	0.002062	0.283069 ± 5	0.283067	6.23	10.51
DB-03		0.067752	0.704218 ± 11	0.704197	0.123710	0.512972 ± 6	0.512955	0.002093	0.283077 ± 6	0.283075	6.52	10.78
DB-07		0.112518	0.706541 ± 3	0.706506	0.125453	0.512889 ± 1	0.512871	0.001932	0.282972 ± 11	0.282970	4.90	7.07
BYCG I-03	1.3–0.11 Ma		0.704213 ± 2			0.512724 ± 4			0.282935 ± 15		1.68	5.78
BYCGII-02	(Ho et al., 2011)		0.704414 ± 3			0.512791 ± 4			0.282881 ± 14		2.98	3.84
BYCGm-05			0.704072 ± 2			0.512857 ± 4			0.282942 ± 12		4.26	6.02
BYCGm-12			0.704112 ± 2			0.512838 ± 5			0.282932 ± 12		3.91	5.65

[a] $^{87}Rb/^{86}Sr$, $^{147}Sm/^{144}Nd$ and $^{176}Lu/^{177}Hf$ are calculated using whole-rock Rb, Sr, Sm, Nd, Lu and Hf contents in Table 1.
[b] $^{87}Sr/^{86}Sr_i = [^{87}Sr/^{86}Sr) - (^{87}Rb/^{86}Sr)(e^{\lambda t} - 1)]$; $^{143}Nd/^{144}Nd_i = [(^{143}Nd/^{144}Nd) - (^{143}Sm/^{144}Nd)(e^{\lambda t} - 1)]$; $^{176}Hf/^{177}Hf_i = [(^{176}Hf/^{177}Hf) - (^{176}Lu/^{177}Hf)(e^{\lambda t} - 1)]$.
[c] $\varepsilon_{Nd}(t) = [(^{143}Nd/^{144}Nd_i) / (^{143}Nd/^{144}Nd_{CHUR}) - 1] \times 10{,}000$; $^{143}Nd/^{144}Nd_{CHUR} = 0.512638$; $\varepsilon_{Hf}(t) = [(^{176}Hf/^{177}Hf_i) / (^{176}Hf/^{177}Hf_{CHUR}) - 1] \times 10{,}000$; $^{176}Hf/^{177}Hf_{CHUR} = 0.282772$.

Fig. 3. The $K_2O + Na_2O$ vs. SiO_2 diagram (Le Maitre, 1989) for Jining basalts, for which, all the data plotted have been normalized to 100% on a volatile-free basis.

samples together with the two literature data (Li et al., 2006) plot away from the field defined by the depleted mid-ocean ridge basalts (MORB) and OIB, but in the field of Paleozoic kimberlite from Mengyin, Shandong province (Zhang et al., 2002, 2008). In $\varepsilon_{Nd}(t)$ vs. $\varepsilon_{Hf}(t)$ diagram (Fig. 8b), the five samples resemble high-Mg andesites from Wulanhada, Liaoning province (Yang et al., 2006).

The 23.5–21.9 Ma basalts also have a large range of $^{87}Sr/^{86}Sr_i$ (0.703602–0.706506), but they have high $\varepsilon_{Nd}(t)$ (4.11–6.52) and high $\varepsilon_{Hf}(t)$ (7.07–10.94). In Fig. 8a, like all other Cenozoic basalts from the east NCC (Basu et al., 1991; Liu et al., 1995a, 1995b; Peng et al., 1986; Song et al., 1990; Zhi et al, 1990), five of the samples plot in the OIB field. However, sample DB-07 shows much higher $^{87}Sr/^{86}Sr_i$. Overall, all the six samples plot in the field defined by clinopyxene separate from the Sanyitang mantle xenoliths (Zhang et al., 2012a). In $\varepsilon_{Nd}(t)$ vs. $\varepsilon_{Hf}(t)$ diagram (Fig. 8b), all the six samples plot in the field defined by the Cenozoic basalts from the east NCC (Yang et al., 2006; Zhang et al., 2012b; Zhu et al., 2012).

The Jining Quaternary basalts show depleted and relatively uniform Sr–Nd–Hf isotopic compositions (i.e., $^{87}Sr/^{86}Sr = 0.704072–0.704414$; $\varepsilon_{Nd} = 1.68–4.26$; $\varepsilon_{Hf} = 3.84–6.02$). These basalts well plot in the field defined by the Cenozoic basalts from the east NCC (Basu et al., 1991; Liu et al., 1995a, 1995b; Peng et al., 1986; Song et al., 1990; Yang et al., 2006; Zhang et al., 2012b; Zhi et al, 1990; Zhu et al., 2012) in both Sr–Nd and Nd–Hf isotope spaces (Fig. 8).

5. Discussion

5.1. Shallow-level processes

5.1.1. Effect of post-magmatic alteration

Most samples of all the three Jining basalt suites are fresh as shown petrographically (Fig. 2), indicated by low LOI values (mostly < 2.0 wt.%; see Table 1), and by the good correlations between abundances of "alteration mobile" elements (e.g., Rb, Ba) and "alteration immobile" elements (e.g., Th, Nb, La, Zr) (Fig. 7). For the Jining 119.6–108.6 Ma basalts, the elevated Rb and Ba contents are not the result of post-magmatic processes, but inherited from the source or source histories. For the Jining 23.5–21.9 Ma basalts, we consider that the anomalously high Rb and Ba in a few samples (Fig. 7a, b) are also inherited from the source (see below). The effect of post-magmatic processes, if any, is limited to Sr and Pb in sample WYF-10 (Fig. 6b), and Pb in sample YYG-18 (Fig. 6d), whose LOI is 2.09 and 1.91, respectively. In summary,

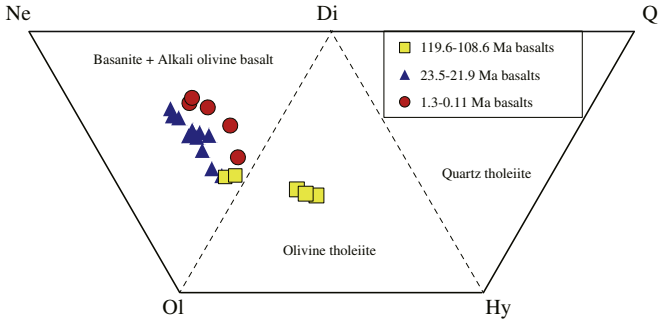

Fig. 4. Normative compositions for Jining basalts. The nomenclature of volcanic rocks followed Yoder and Tilley (1962).

post-magmatic processes may have affected only Sr and Pb in a few samples, which will not affect our petrogenetic interpretations for these rock suites (see below).

5.1.2. Crustal contamination

The NCC crust is characterized by elevated abundances of SiO_2 (61.9 wt.% on average) and large ion lithophile elements (LILEs; e.g., Rb, Ba, Th, U), depletion of high field strength elements (HFSEs; e.g., Nb, Ta) (Gao et al., 1998) with high $^{87}Sr/^{86}Sr$ and low $^{143}Nd/^{144}Nd$ (Liu et al., 2004). Thus, if there were significant crustal contamination, the LILE/HFSE ratios and $^{87}Sr/^{86}Sr$ of these basalts would positively correlate with SiO_2, while the $^{143}Nd/^{144}Nd$ would negatively correlate with SiO_2.

In Th/Nb vs. SiO_2 and U/Ta vs. SiO_2 diagrams (Fig. 9a, b), the Th/Nb and U/Ta ratios are essentially constant for all three basalt suites, which is consistent with insignificant crustal contamination. Furthermore, the absence of positive $^{87}Sr/^{86}Sr_i$–SiO_2 (Fig. 9c) and negative $\varepsilon_{Nd}(t)$–SiO_2 (Fig. 9d) correlations for 119.6–108.6 Ma basalts and 1.3–0.11 Ma basalts also suggest insignificant crustal assimilation. Such conclusion is supported by several other lines of evidence:

(1) As discussed above, all the three basalt suites have positive Nb and Ta anomalies in the spidergram (Fig. 6b, d, f). Fig. 10 further illustrates that all the three basalt suites have far more higher

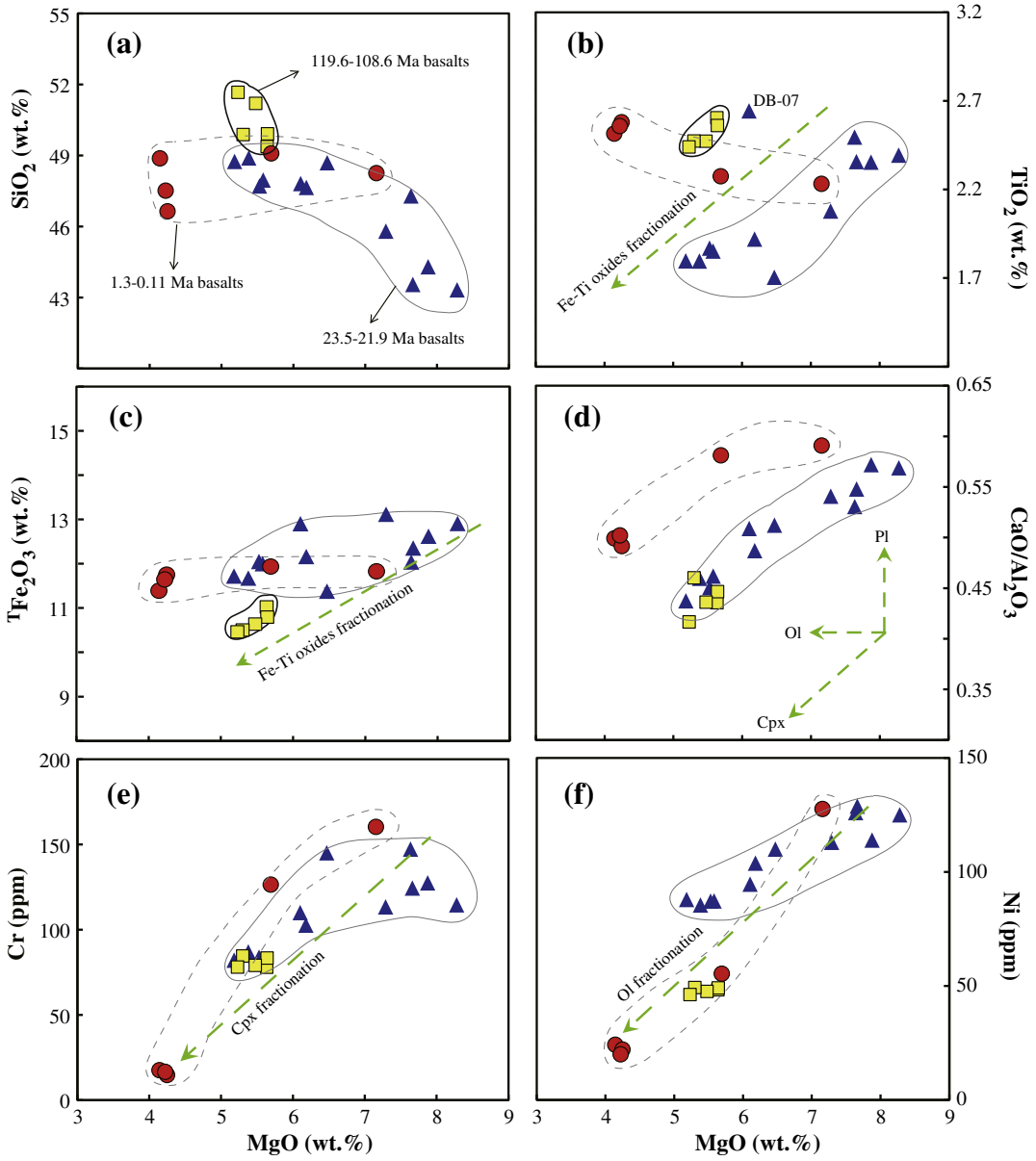

Fig. 5. MgO-variation diagrams showing major element oxides, CaO/Al_2O_3, Cr and Ni for Jining basalts. Arrows with decreasing MgO indicate the fractional crystallization trends.

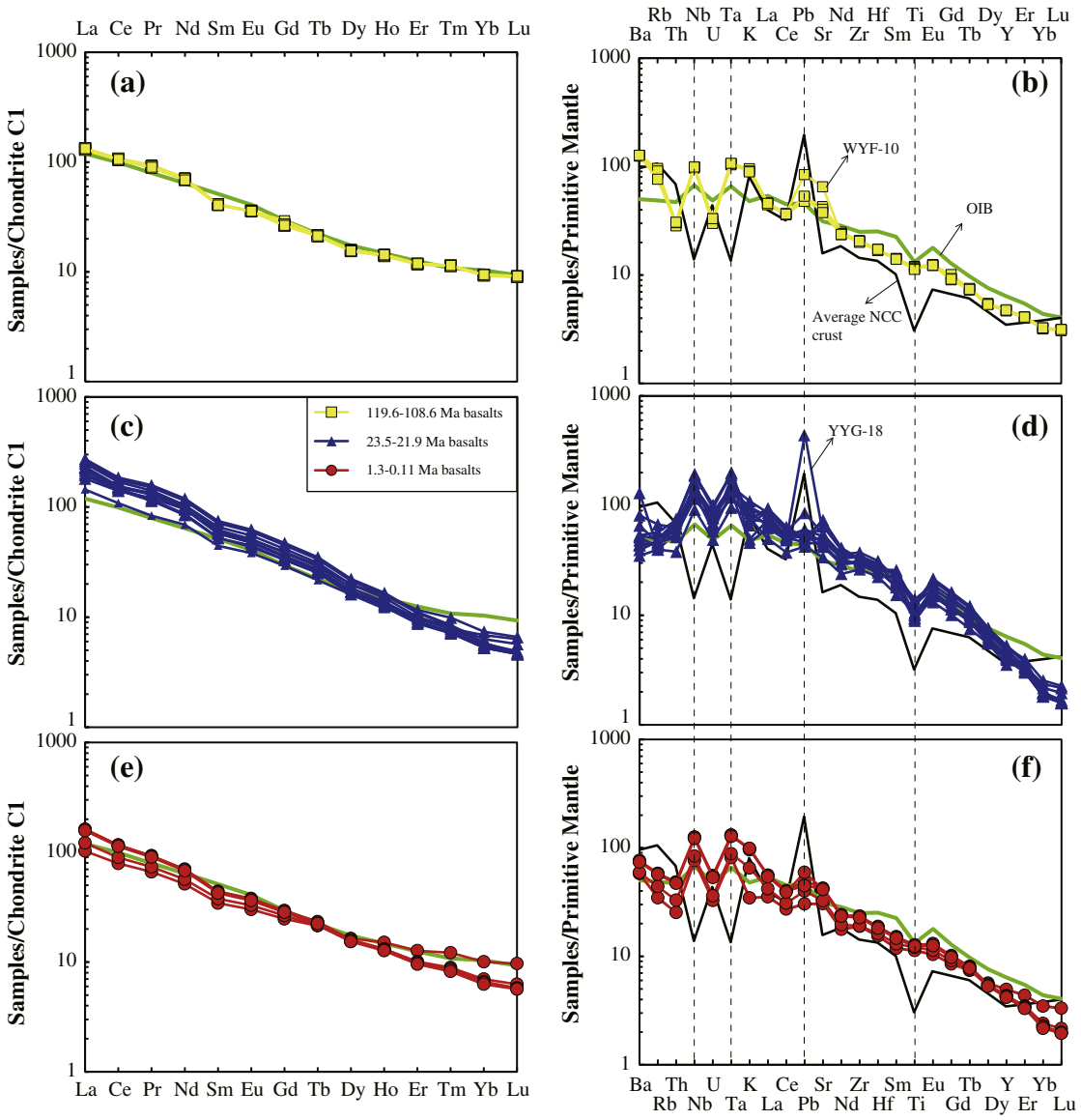

Fig. 6. Chondrite-normalized rare earth element and primitive mantle normalized incompatible element patterns for the Jining basalts. For comparison, average composition of ocean island basalts (OIB; Sun and McDonough, 1989) and the average NCC crust (Gao et al., 1998) are also plotted. Chondrite and primitive mantle values are from Sun and McDonough (1989).

$[Nb/Th]_{PM}$ and $[Ta/U]_{PM}$ than the NCC continental crust (Gao et al., 1998), which is consistent with negligible crustal contamination.

(2) Nb/U ratio ranges are: 101.4–109.7 for the 119.6–108.6 Ma basalts, 55.8–84.6 for the 23.5–21.9 Ma basalts, and 76.7–79.1 for the Quaternary basalts, which are all significantly higher than those of MORBs and OIBs ($Nb/U = 47 \pm 10$; Hofmann et al., 1986). Because the Nb/U ratio of the NCC continental crust is low (10.6; Gao et al., 1998), addition of an insignificant amount of continental material to the erupted magma would have affected this elemental ratio.

(3) For the 23.5–21.9 Ma basalts, although there is a weak negative correlation between $\varepsilon_{Nd}(t)$ and SiO_2 (Fig. 9d), the presence of mantle xenoliths in both Dongba basalts and Youyinggou basalts, which is consistent with the interpretation of rapid ascent of magma and thereby having limited crustal residence (Sun et al., in preparation), argue again that the contamination is limited. Note that the sample DB-07 has relatively higher $^{87}Sr/^{86}Sr_i$ and lower $\varepsilon_{Nd}(t)$. We consider that such a Sr–Nd isotopic characteristic was not caused by contamination of the continental crust, but was inherited from the magma source (see details below).

5.1.3. Fractional crystallization

As all three Jining basalt suites show insignificant crustal assimilation/contamination, the highly evolved characteristics with low $Mg^{\#}$ ($Mg / [Mg + Fe^{2+}]$): 0.52–0.53 for the 119.6–108.6 Ma basalts, 0.49–0.59 for the 23.5–21.9 Ma basalts and 0.44–0.57 for the Quaternary basalts, suggest that their extensive fractional crystallization dominated melt evolution prior to eruption.

Despite the restricted variation of MgO for the 119.6–108.6 Ma basalts, the apparent positive correlations between TiO_2, $^{T}Fe_2O_3$ and MgO (Fig. 5b, c) suggest Fe–Ti oxides crystallization from the magma, which is consistent with the petrographic observations (Fig. 2a).

On MgO variation diagrams (Fig. 5), the 23.5–21.9 Ma samples form a negative trend in SiO_2–MgO space and positive trends in CaO/Al_2O_3–MgO, Cr–MgO and Ni–MgO spaces, which are consistent with fractional crystallization dominated by olivine and clinopyroxene as the major liquidus phases at high pressures. Note that the decreasing TiO_2 with decreasing MgO from 8.28 wt.% to 5.18 wt.% is inconsistent with the familiar late appearance (i.e., T = ~1100 °C; Niu et al., 2002b) of Ti–Fe oxides (ilmenite–magnetite solid solutions) at low pressures. The positive TiO_2–MgO correlation here may suggest Ti-rich parental magmas

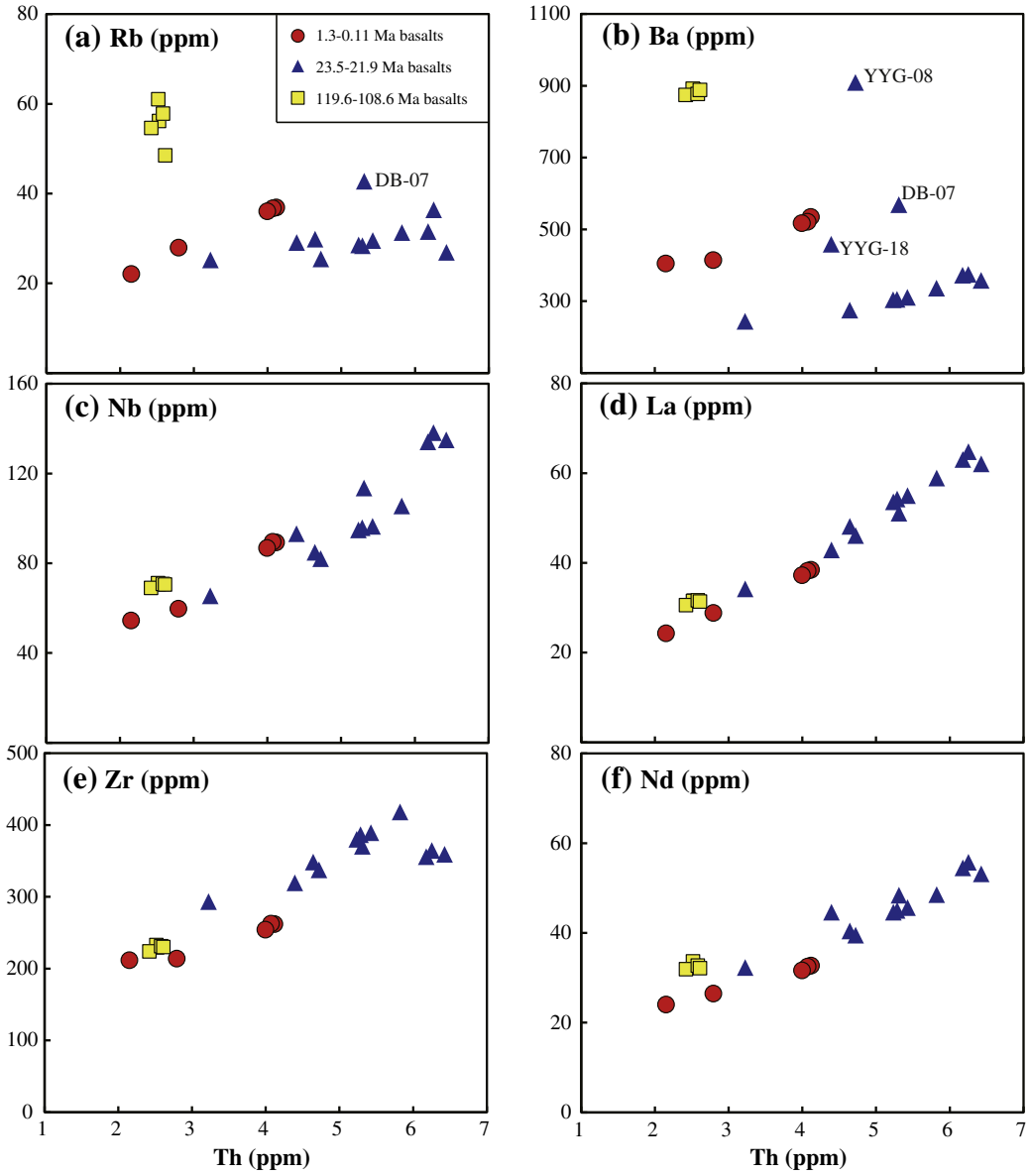

Fig. 7. Variation of selected trace element versus Th for the Jining basalts.

with high oxygen fugacity that begins to crystallize Fe–Ti oxides (ilmenite or pseudobrookite) at higher temperatures (e.g., Charlier et al., 2009). This would be consistent with the correspondingly rapid SiO_2 increase with decreasing MgO because Fe–Ti oxides contain little SiO_2. This would also be consistent with magma chambers present in the lithospheric mantle conditions (14.1–23.5 kbar; Sun et al., in preparation).

Despite limited number of samples, the Jining Quaternary basalts display a relatively large MgO variation range with correlated variations that are consistent with olivine and clinopyroxene dominated fractional crystallization at high pressures. This TiO_2 increase with decreasing MgO suggests relatively low TiO_2 parental magmas with probably low oxygen fugacity that begins to crystallize Fe–Ti oxides at lower temperatures (Fig. 5). Well-designed crystallization experiments on alkali basalts with varying volatile contents and oxygen fugacity under lithospheric mantle conditions will be needed to test this hypothesis.

5.2. Petrogenesis of 119.6–108.6 Ma basalts

As we have demonstrated above that crustal contamination and post-magmatic alteration were rather insignificant for these basalts, we can thus discuss their petrogenesis in terms of mantle sources and source histories as well as melting conditions.

The 119.6–108.6 Ma basalts have elevated abundances of incompatible elements, strongly fractionated REE patterns with high LREE/HREE ratios (Fig. 6a, b), and enriched isotopic signatures with high $^{87}Sr/^{86}Sr_i$, low $\varepsilon_{Nd}(t)$ and low $\varepsilon_{Hf}(t)$ (Table 2 and Fig. 8a, b). They are isotopically more enriched than most of the present-day OIB as shown in Sr–Nd isotope space (see Fig. 8a). Importantly, these 119.6–108.6 Ma basalts from the west NCC are still far less enriched than the 125 Ma Fangcheng basalts from the east NCC (Zhang et al. 2002; see Fig. 8). Such isotopically moderately enriched signatures could result from: (1) mantle sources with components of recycled sediments; (2) partial melting of ancient metasomatized lithospheric mantle.

Because sediments have higher Pb and lower Nb and Ta (Plank and Langmuir, 1998) than OIB, it would impart such signatures in the erupted basalts if recycled sediments were indeed the enriched components in the source (Niu et al., 2012), which is not observed in the 119.6–108.6 Ma basalts (Fig. 6b). Thus we prefer explanation (2), which is supported by the existence of old lithospheric relicts in the uppermost mantle beneath the west NCC, recognized recently through

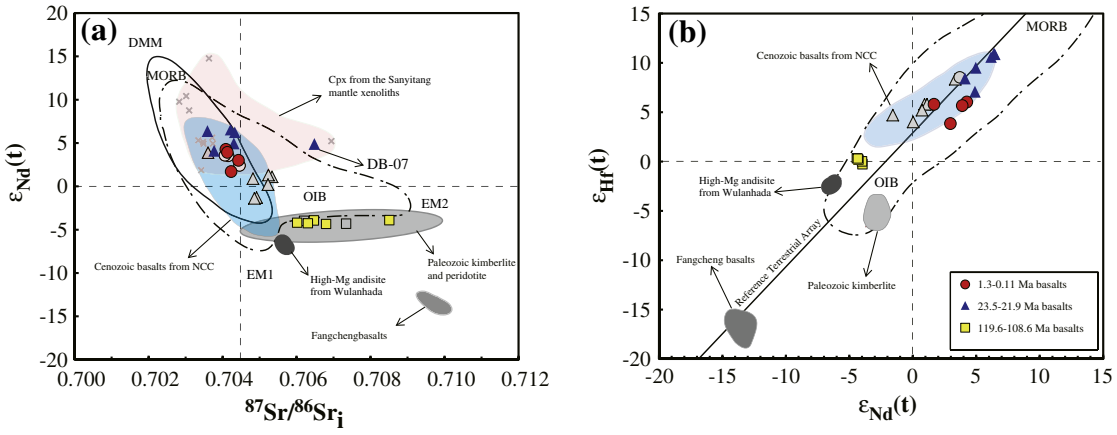

Fig. 8. (a) Sr and Nd isotope compositions of the Jining basalts. For comparison, Paleozoic kimberlite and peridotite from Mengyin, Mesozoic basalts from Fangcheng (Zhang et al., 2002), Cenozoic basalts from east NCC (Basu et al., 1991; Liu et al., 1995a, 1995b; Peng et al., 1986; Song et al., 1990; Zhi et al, 1990), Wulanhada high-Mg andisites (Zhang et al., 2003) in the literature are also plotted. Sr and Nd isotope data for the clinopyroxene that separates from lherzolite xenoliths in the Sanyitang basalts (Zhang et al., 2012a) are also shown for comparison. The two 119.6–108.6 Ma basalt data (gray solid squares) are from Li et al. (2006). The literature data for 23.5–21.9 Ma basalts (gray solid triangle) and the Quaternary basalts (gray solid circles) are from Ho et al. (2011) and Zhang et al. (2012b). (b) $\varepsilon_{Nd}(t)$ vs. $\varepsilon_{Hf}(t)$ diagram for the Jining basalts. The data source for Mesozoic basalts from Fangcheng, Wulanhada high-Mg andesites, Paleozoic kimberlite and peridotite from Mengyin, the Jining 23.5–21.9 Ma basalts and Jining Quaternary basalts are the same as in (a), the Hf isotope data for NCC Cenozoic basalts are from Yang et al. (2006), Zhu et al. (2012), and Zhang et al. (2012b). Reference Terrestrial Array ($\varepsilon_{Hf} = 1.36\varepsilon_{Nd} + 2.95$) is after Vervoort and Blichert-Toft (1999).

Sr–Nd–Os isotope studies of mantle xenoliths hosted in the Sanyitang Miocene basalts (Zhang et al., 2012a).

Assuming that the NCC had similar lithosphere history with similar lithospheric mantle composition before the east NCC lithosphere had been thinned, then the ancient lithospheric mantle is expected to be similar beneath east and west NCC in terms of Sr–Nd–Hf isotopes. Indeed, in Sr–Nd isotope space, the Jining 119.6–108.6 Ma basalts plot in the field of NCC old lithosphere mantle (Zhang et al., 2002, 2008), providing evidence that the source of these basalts may be metasomatized lithospheric mantle. Furthermore, these isotopic features are also similar to those of Mesozoic high-Mg andesites in Wulanhada (Fig. 8), whose source is interpreted as metasomatically enriched mantle material

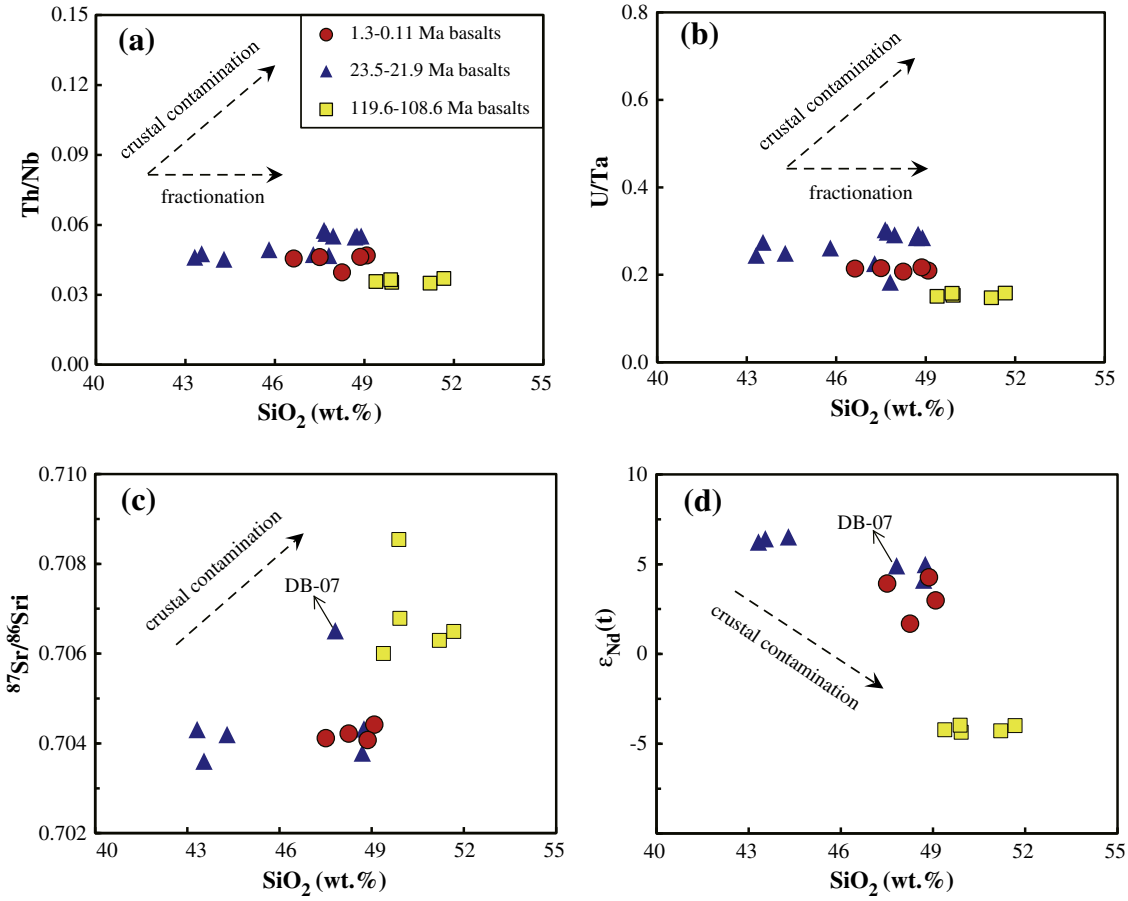

Fig. 9. (a) Th/Nb vs. SiO_2, (b) U/Ta vs. SiO_2, (c) $^{87}Sr/^{86}Sr$ vs. SiO_2 and (d) $\varepsilon_{Nd}(t)$ vs. SiO_2 diagrams for Jining basalts to illustrate negligible crustal contamination before eruption.

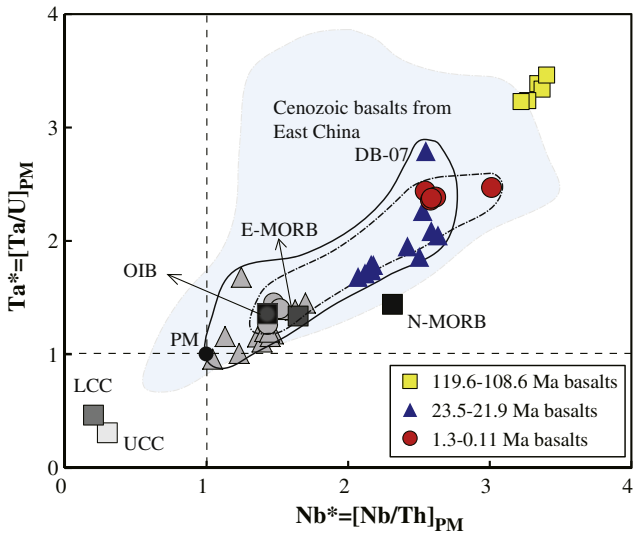

Fig. 10. (a) Nb*([Nb/Th]$_{PM}$) vs. Ta*([Ta/U]$_{PM}$) diagram (Niu and Batiza, 1997) for the Jining basalts to illustrate negligible crustal contamination during magma ascent through crust to the surface. It also shows that the 23.5–21.9 Ma and 1.3–0.11 Ma Jining basalts share a similar enriched magma source in terms of Nb and Ta. LCC and UCC are, respectively, average composition of the lower and upper crust of the NCC (Gao et al., 1998); PM denotes primitive mantle (Sun and McDonough, 1989). The literature data for 23.5–21.9 Ma basalts (gray solid triangle) and the Quaternary basalts (gray solid circles) are from Ho et al. (2011) and Zhang et al. (2012b).

(Yang et al., 2006; Zhang et al., 2003). Thus, taking both isotope (Fig. 8) and trace element systematics (Fig. 6a, b) together, we propose that the Jining 119.6–108.6 Ma basalts are most consistent with an origin of partial melting of metasomatized lithospheric mantle.

The mantle metasomatism has been a long held concept used to explain the geochemically enriched signatures of the cratonic lithospheric mantle (e.g., Hawkesworth et al. 1990; Lloyd and Bailey, 1975), and such enriched (metasomatized) lithospheric mantle has been considered as one important source reservoir for alkalic volcanism (Furman, 1995; Guo et al., 2014; Hawkesworth et al. 1990; Niu, 2008; Pilet et al., 2008). In the context of the global OIB petrogenesis, Niu and co-authors proposed that the contact between the growing oceanic lithosphere and the subjacent asthenosphere (or seismic low velocity zone i.e., LVZ) is the most likely location of mantle metasomatism because of the presence of low-degree (low-F) melt highly enriched in volatiles and incompatible elements in the LVZ (Niu and O'Hara, 2003, 2009; Niu et al., 2012). The ultimate source of the low-F melt can be internally generated under the conditions of the LVZ (Niu, 2008) or subducted seafloor materials including terrigenous sediments and carbonaceous sediments (Guo et al., 2014). The subducted ocean crust is expected to be enriched in Nb (vs. Th) and Ta (vs. U) after going through subduction dehydration (Niu and Batiza, 1997; Niu et al., 2002a), which, along with carbonaceous sediments, can produce low-F melt to metasomatize the deep portions of the cratonic lithosphere. Apart from the low-F melt, veins of pyroxenite and hornblendite formed during the lithosphere growth also play an important role in the petrogenesis of OIB (Niu, 2008; Niu et al., 2012; Pilet et al., 2008, 2010). The above interpretations and reasoning may also be true beneath the cratonic lithosphere in its history. Melting of such ancient metasomatized lithospheric mantle will give rise to melts of enriched isotopic signatures and trace element systematics with high [Nb/Th]$_{PM}$ and [Ta/U]$_{PM}$ as the Jining 119.6–108.6 Ma basalts show (Figs. 6a, b, 8 and 10).

5.3. Petrogenesis of Jining 23.5–21.9 Ma basalts

The 23.5–21.9 Ma basalts have low $^{87}Sr/^{86}Sr_i$ (0.703602–0.706506), high $\varepsilon_{Nd}(t)$ (4.11–6.52) and high $\varepsilon_{Hf}(t)$ (7.07–10.94) as Cenozoic basalts from eastern China studied previously (Basu et al., 1991; Ho et al., 2011;

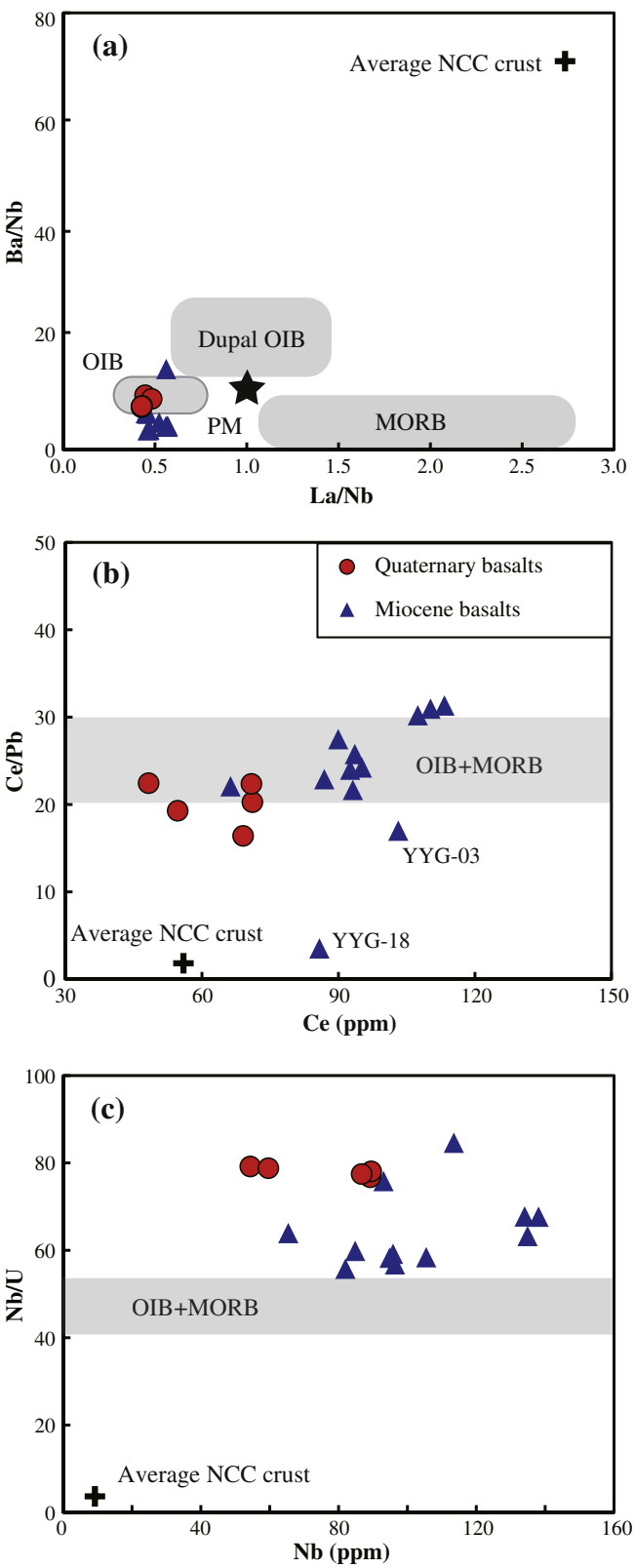

Fig. 11. (a) Ba/Nb vs. La/Nb, (b) Ce/Pb vs. Ce, and (c) Nb/U vs. Nb diagrams for the Jining basalts, showing the 23.5–21.9 Ma and 1.3–0.11 Ma Jining basalts originated from enriched asthenospheric mantle. Field for mid-ocean ridge basalts (MORB), ocean island basalts (OIB), Dupal OIB, and primitive mantle (PM) in (a) are after Wilson (1989) and the average NCC crust is after Gao et al. (1998). The average ratios of Nb/U and Ce/Pb in OIB and MORB are after Hofmann et al. (1986).

Yang et al., 2006; Zhang et al., 2012b; Zhu et al., 2012), and plot in the OIB field in $^{87}Sr/^{86}Sr_i$–$\varepsilon_{Nd}(t)$ and $\varepsilon_{Nd}(t)$–$\varepsilon_{Hf}(t)$ spaces (Fig. 8; except the sample DB-07 with higher $^{87}Sr/^{86}Sr_i$), suggesting that they may have similar origin, i.e., partial melting of asthenosphere. The observations below can provide further evidence to support this interpretation: (1) Their Ba/Nb and La/Nb ratios range from 2.65 to 11.09 and 0.45 to 0.57, respectively, overlapping the present-day OIB (see Fig. 11a); (2) the Ce/Pb ratios of 23.5–21.9 Ma basalts are within the range defined by OIB + MORB (Figs. 11b; Hofmann et al., 1986), and the Nb/U ratios for the 23.5–21.9 Ma basalts are significantly higher than the values for OIB + MORB (Fig. 11c; Hofmann et al., 1986); (3) Chen et al. (2009) and Chen (2010) suggested that lithospheric thickness along the Yinchuan–Hetao and Shaanxi–Shanxi rift areas is as thin as ~80 km at present. The elevated $[La/Yb]_N$ (21.1–47.0) and especially the high $[Sm/Yb]_N$ (3.88–6.34) for the Jining 23.5–21.9 Ma basalts are consistent with melt generation in the garnet lherzolite stability field. If the defined garnet-spinel face boundary near the solidus condition is ~85 km deep (Robinson and Wood, 1998), then the melting region for the Jining 23.5–21.9 Ma basalts should be in the asthenosphere with the base of the lithosphere not significantly shallower than ~85 km because otherwise decompression melting in the spinel lherzolite stability field would be significant and will lower the $[Sm/Yb]_N$ in the erupted basalts (Niu et al., 2011).

Importantly, Jining 23.5–21.9 Ma basalts have an enriched characteristic with elevated abundances of incompatible elements (Fig. 6c, d), together with the high $[La/Yb]_N$, reflect their derivation from an enriched fertile mantle source. The decoupling of significantly enriched incompatible element signature (Fig. 6c, d) with low $^{87}Sr/^{86}Sr$, high $^{143}Nd/^{144}Nd$ and high $^{176}Hf/^{177}Hf$ isotope ratios (Fig. 8), therefore, suggests that low-degree (low-F) melt metasomatism must have taken place in no distant past in the magma source region before melting for the 23.5–21.9 Ma basalts.

As mentioned above, the lithosphere–asthenosphere boundary (LAB) is the most likely location of mantle metasomatism (Niu and O'Hara, 2003; Niu et al., 2011). In addition to fertile mantle source material from depth, OIB melts may have the contribution of the low-F melt (highly enriched in volatiles and incompatible elements) at top of the LVZ and the metasomatic veins formed earlier in the lithosphere (Niu and O'Hara, 2003; Niu et al., 2011). Such a model can also explain the petrogenesis of OIB-like continental basalts such as Cenozoic basalts from eastern China. Thus, we propose that the Jining 23.5–21.9 Ma basalts, as well as Cenozoic basalts from eastern China, were produced by partial melting of such metasomatized LVZ beneath the NCC. This can well account for the highly enriched incompatible elements signatures as well as the low $^{87}Sr/^{86}Sr_i$, high $\varepsilon_{Nd}(t)$ and high $\varepsilon_{Hf}(t)$ in both the Jining 23.5–21.9 Ma basalts and Cenozoic basalts from eastern China.

Note that sample DB-07 has obviously higher $^{87}Sr/^{86}Sr_i$ than other samples. But this sample also possesses the highest $[Ta/U]_{PM}$ (Fig. 10), precluding the possibility of contribution of terrigenous sediments. Therefore, we suggest that the high $^{87}Sr/^{86}Sr_i$ of DB-07 should be the result of assimilation of time-integrated metasomatic veins, which were characterized by the high Rb/Sr ratio, formed early in the history of the lithospheric mantle. This is consistent with this sample (DB-07) having the highest Rb/Sr ratio among all the 23.5–21.9 Ma samples. The $^{87}Sr/^{86}Sr_i$ of 23.5–21.9 Ma samples within the range of clinopyroxene separates from the lherzolite xenoliths in Sanyitang Cenozoic basalts (Fig. 8a; Zhang et al., 2012a) may also reflect the contribution of lithospheric mantle to these samples. In addition, the high Ba content in DB-07 (also samples YYG-08 and YYG-18) is most likely related to the subducted carbonaceous sediments in the first place (Guo et al., 2014).

We interpret the Jining 23.5–21.9 Ma basalts resulted from partial melting of metasomatized asthenosphere or LVZ beneath the NCC, but the question concerns the origin of the low-F melt. Fig. 10 illustrates that the Jining 23.5–21.9 Ma basalts, like Cenozoic basalts from eastern China, possess excess Ta (vs. Th) and Nb (vs. U). Niu and coworkers found $D_{Nb} \approx D_{Th} < D_{Ta} \approx D_U$ (Niu and Batiza, 1997; Niu et al., 2002a) in basalts from East Pacific Rise (EPR) and considered such excess Ta and Nb in lavas must be inherited from previous metasomatic events. They further speculated that the subduction-zone dehydration metamorphic reactions are the only known process that can effectively fractionates Nb from Th, and Ta from U. Thus, the ultimate source of the low-F melt (or metasomatic agent) could be subducted seafloor materials including terrigenous and carbonaceous sediments (Guo et al., 2014; Niu and Batiza, 1997; Niu and O'Hara, 2003). This may be more likely the case for the Cenozoic basaltic magmatisms in eastern China, because the subducted Paleo-Pacific slab lying in the mantle transition zone (410–660 km) beneath the region could be the best source of fluids and hydrous melts (Kuritani et al., 2011; Niu, 2005; Sakuyama et al., 2013), i.e., the low-F melt (metasomatic agent) to metasomatize the deep portions of the cratonic lithosphere and LVZ. This process can explain the petrogenesis of the Jining 23.5–21.9 Ma basalts in particular, also the petrogenesis of the Cenzoic basalts from eastern China in general.

5.4. Petrogenesis of Jining Quaternary basalts

The Quaternary basalts (1.3–0.11 Ma) display low $^{87}Sr/^{86}Sr$ ratios (0.704072–0.704414), high ε_{Nd} (1.68–4.26) and high ε_{Hf} (3.84–6.02) as the Jining 23.5–21.9 Ma basalts and plot in the field defined by those of the 23.5–21.9 Ma basalts in $^{87}Sr/^{86}Sr_i$–$\varepsilon_{Nd}(t)$ (Fig. 8a) and $\varepsilon_{Nd}(t)$–$\varepsilon_{Hf}(t)$ spaces (Fig. 8b). These basalts also have an enriched characteristic with elevated incompatible element abundances (Fig. 6e, f), indicating their derivation from an incompatible element enriched fertile mantle source. We suggest that the Jining Quaternary basalts shared a very similar enriched asthenospheric mantle origin with the 23.5–21.9 Ma basalts. The observations below can provide further evidence for such a conclusion: (1) As mantle melting does not fractionate Nb from Th, nor Ta from U (Niu and Batiza, 1997; Niu et al., 2002a), the $[Nb/Th]_{PM}$ and $[Ta/U]_{PM}$ could, therefore, well reflect their magma source before melting occurred, i.e., any Ta and Nb anomalies in lavas must be a source signature inherited from previous events. Fig. 10 shows that the Quaternary basalts, together with the literature data (Ho et al., 2011; Zhang et al., 2012b), basically plot in the field of the 23.5–21.9 Ma basalts in the $[Nb/Th]_{PM}$ vs. $[Ta/U]_{PM}$ diagram, indicating that they share a similar enriched asthenospheric mantle source; (2) Fig. 11a illustrates that the Quaternary basalts plot within the 23.5–21.9 Ma basalt field in La/Nb vs. Ba/Nb diagram; the Ce/Pb and Nb/U ratios for the Jining Quaternary basalts also plot in the ranges of the 23.5–21.9 Ma basalts (Fig. 11b, c).

Despite the similar origin, there are also differences between the Quaternary basalts and the 23.5–21.9 Ma basalts. For example, the Quaternary basalts show basically lower moderately/weakly incompatible element ratios than the 23.5–21.9 Ma basalts (Fig. 12). Now that these two stages of volcanism have very similar asthenosphere source, the differences of moderately/weakly incompatible elements ratios, thus, most probably result from varying extent of melting. Niu et al. (1996) found that moderately/weakly incompatible element ratio is much more sensitive to the extent of melting than involving highly incompatible elements. Thus, the lower moderately/weakly incompatible element ratios for the Jining Quaternary basalts (Fig. 12) may qualitatively suggest their derivation from a greater extent of melting than the Jining 23.5–21.9 Ma basalts.

The differences in ratios of moderately/weakly incompatible elements between the 23.5–21.9 Ma basalts and the Quaternary basalts effectively demonstrate that the lithosphere thickness control the geochemistry of erupted basaltic melts, i.e., the "lid effect" (Niu et al., 2011). Explicitly, the petrogenesis of the 23.5–21.9 Ma basalts represents asthenospheric melting and melt extraction beneath the thinned lithosphere, but the Jining Quaternary basalts reflect melting beneath the even thinner lithosphere. The 23.5–21.9 Ma basalts and the Quaternary basalts both reflect the asthenospheric melting that began in the

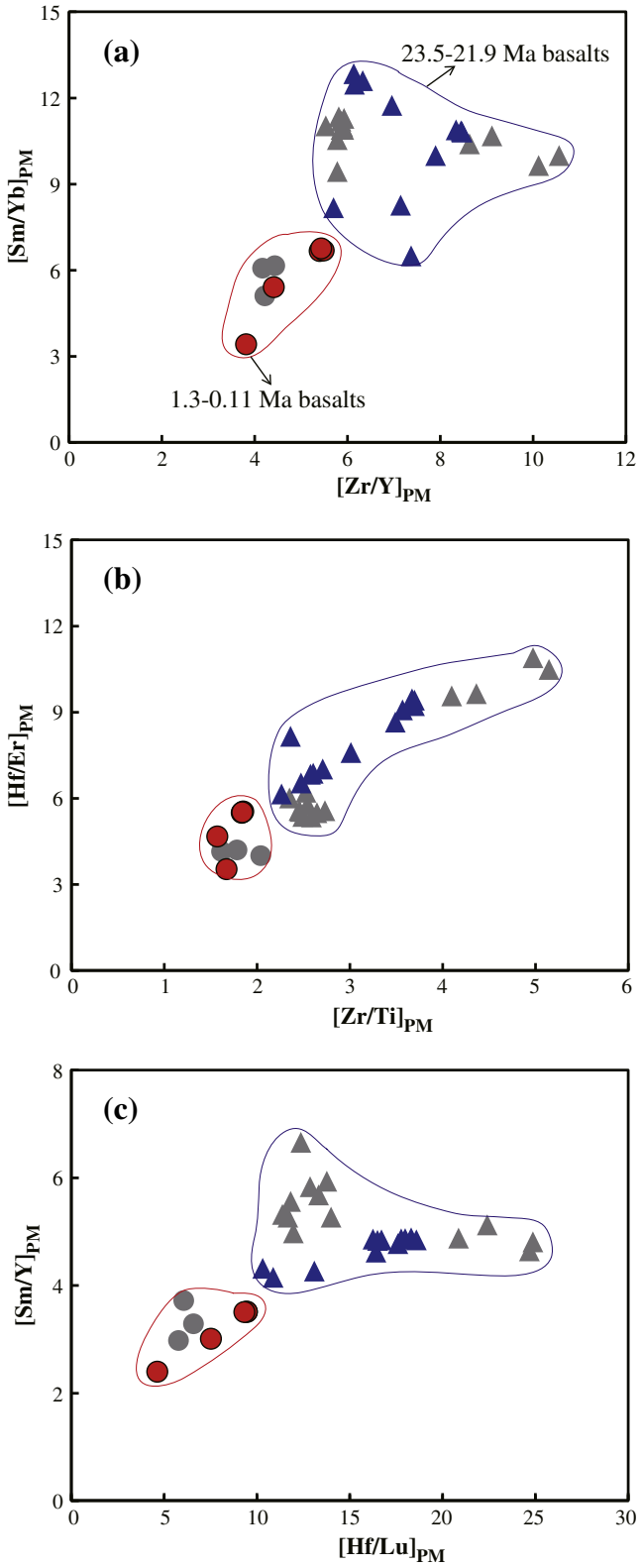

Fig. 12. (a) $[Sm/Yb]_{PM}$ vs. $[Zr/Y]_{PM}$, (b) $[Hf/Er]_{PM}$ vs. $[Zr/Ti]_{PM}$ and (c) $[Sm/Y]_{PM}$ vs. $[Hf/Lu]_{PM}$ diagrams to show that the Jining 23.5–21.9 Ma basalts reflect a smaller degree partial melting of asthenospheric mantle than the Jining Quaternary basalts.

garnet lherzolite stability field, but the final depth of melting for the Quaternary basalts is shallower with thinner lithosphere. This is well reflected by the dilution of the low-F melting signature (i.e., lower abundances of incompatible elements) and the weaker "garnet signature" (e.g., lower $[Sm/Yb]_N$) for the Quaternary basalts with greater extent of melting in the spinel peridotite stability field (see Niu et al., 2011 for details). This concept is elaborated below.

5.5. Lithosphere thinning in west NCC

As mentioned above, the west NCC and the east NCC should not have big differences in both the lithosphere thickness and other lithosphere properties (e.g., lithology) since the collision between east and west blocks at 1.8 Ga (Zhao et al., 2001). Despite the lack of diamondiferous kimberlite occurrence in the west NCC, the lithosphere thickness is theoretically no less than ~200 km before thinned in the Mesozoic. Chen et al. (2009) and Chen (2010) suggested that lithosphere thickness beneath the Ordos Block is ~200 km at present, while the lithospheric thickness under the late Cenozoic Yinchuan–Hetao and Shaanxi–Shanxi rift areas is as thin as ~80 km. Therefore, the lithosphere under west NCC must have been thinned, at least on local scales (e.g., Yinchuan–Hetao area, Shaanxi–Shanxi rift area).

The change from an old, cold, thick and fertile "cratonic" lithospheric mantle to a young, hot, thin and depleted oceanic-like lithospheric mantle (Griffin et al., 1998; Menzies et al., 1993) was proposed to illustrate the lithosphere thinning of the NCC. DePaolo and Daley (2000) and Xu (2001) also considered the lithosphere change from an enriched mantle to a depleted one as an indicator of lithospheric thinning. Niu (2005) suggested that the lithosphere thinning of the NCC is actually a process that the lithospheric mantle transformed into the asthenospheric mantle. For the west NCC, this is expressed by the Jining 119.6–108.6 Ma basalts with high $^{87}Sr/^{86}Sr_i$, low $\varepsilon_{Nd}(t)$ and $\varepsilon_{Hf}(t)$, which is considered to be the result of partial melting of ancient fertile lithospheric mantle, and by the Quaternary basalts of asthenosphere origin with low $^{87}Sr/^{86}Sr$, high ε_{Nd} and ε_{Hf} (Fig. 8a, b). The distribution of the Jining basalts, as well as other nearby basalts in this region (e.g., Ho et al., 2011; Zhang and Han, 2006; Zhang et al., 2012b), confined within this region of thinned lithosphere in the west NCC (Chen, 2010; Chen et al., 2009; Xu et al., 2004), is also evidence that lithosphere under the west NCC had been thinned on local scales.

Recent observations (Humphreys and Niu, 2009; Niu et al., 2011) demonstrate that on a global scale, the intra-plate ocean island basalts show compositional variation that is, in simple clarity, consistent with the lithosphere thickness variation, i.e., the lithosphere thickness controls the composition of the erupted basalts or the "lid effect" (Ellam, 1992; Niu et al., 2011). That is, the extent of melting is lower beneath the thicker lithosphere with the melt having higher abundances of incompatible elements and stronger garnet signature than beneath the thinner lithosphere. Niu et al. (2011) suggested that the concept of the "lid effect" also applies to the petrogenesis of basalts erupted in continental settings. As shown above, the Jining Miocene basalts of 23.5–21.9 Ma display a lower degree of partial melting signature with greater garnet signature relative to the Jining Quaternary basalts (Fig. 12), which means that the lithosphere thickness during the 23.5–21.9 Ma volcanism is thicker than that in the Quaternary.

5.6. Geodynamics

5.6.1. The geodynamics of lithosphere thinning and the early Cretaceous volcanism in the west NCC

Consensus has been reached in recent years that the east NCC lost its ancient subcontinental lithospheric mantle (SCLM) roots during the Mesozoic, and its thickness has been reduced from more than ~200 km in the Paleozoic to less than ~80 km at present (Fan et al., 2000; Gao et al., 2002; Griffin et al., 1998). In contrast, the SCLM beneath the west NCC remains thick (Deng et al., 2004). However, our study and the high-resolution seismic studies of the NCC (e.g., Chen et al., 2009; Chen, 2010) show that the lithosphere thinning did occur locally in the west NCC and this lithosphere thinning continues to the present

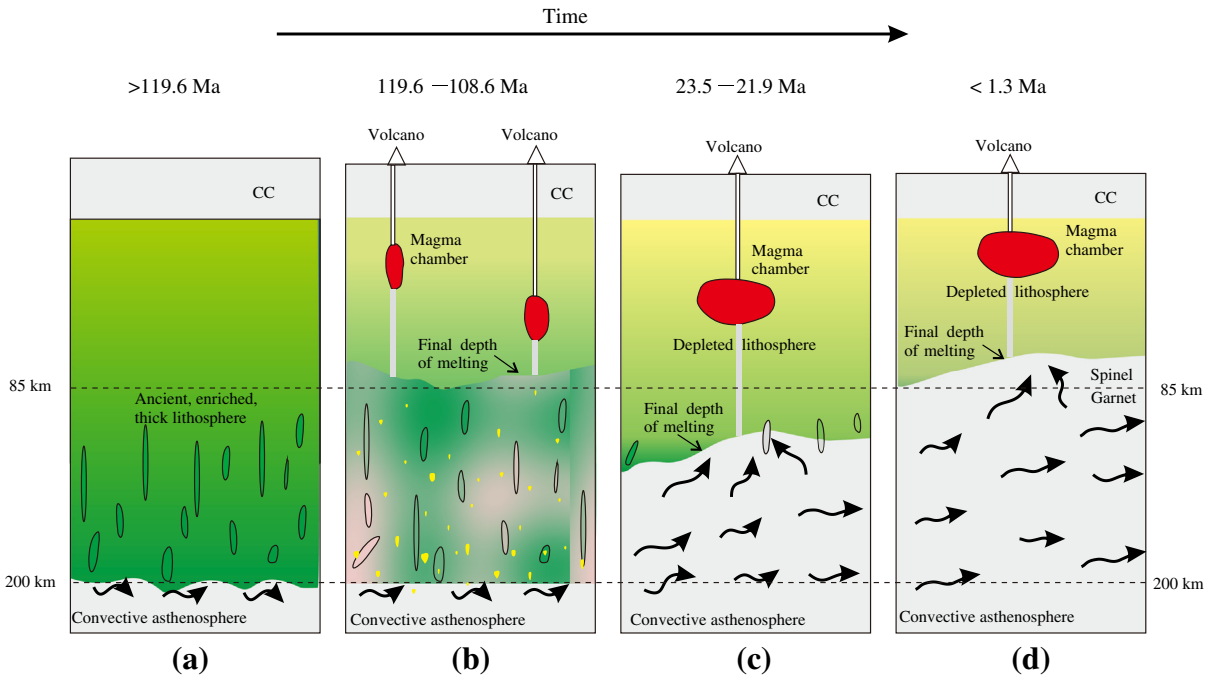

Fig. 13. (a) Illustrates the ancient enriched lithospheric mantle beneath the western NCC was very thick with enriched metasomatic veins present in the deep portion; (b) the water (most likely hydrous melt; yellow dots) released from the Paleo-Pacific slab induced partial melting of lower part of ancient enriched lithosphere, resulting in the 119.6–108.6 Ma volcanism. (c) The lithosphere underneath has thus been thinned from 119.6–108.6 Ma to 23.5–21.9 Ma with the enriched/metasomatized deep portions removed and occupied by the new asthenospheric materials. The melt generated from partial melting of such asthenosphere, sometimes assimilating the metasomatic veins within overlying lithosphere during ascent, produced the 23.5–21.9 Ma Jining basalts. (d) The Jining Quaternary basalts (1.3–0.11 Ma) represent the products derived from asthenosphere beneath the thinned and thus thinner lithosphere than during 23.5–21.9 Ma magmatism. (For interpretation of the references to color in this figure legend, the reader is referred to the web version of this article.)

(Niu, 2014). What may have caused the lithosphere thinning and the extensive volcanism in the Mesozoic and Cenozoic?

Deng et al. (1998) proposed mantle plumes as being responsible for the destruction of the NCC and the large scale of volcanism since the Mesozoic. However, the horizontal "cold" slab in the transition zone beneath eastern China (Kárason and Van der Hilst, 2000; Zhao, 2009) as a cold thermal boundary layer prevents any thermal mantle plumes coming up from the lower mantle, nor favor the initiation of hot thermal plumes from within-upper mantle (Niu, 2005). The absence of mantle plumes under the NCC does not support the thermal–mechanical erosion model (Griffin et al., 1998; Menzies et al., 1993; Xu, 2001) because this model needs extra heat that is unavailable. Furthermore, the thermal–mechanical erosion model describes a gradual, long-lived process, which is inconsistent with lithosphere thinning related magmatism that may have taken place in a relatively short period of 135–115 Ma (Wu et al., 2008). Lithosphere delamination is another model invoked to explain the lithosphere thinning in the NCC (Gao et al., 2004, 2009; Xu et al., 2006). While this interpretation is attractive, it is physically not straightforward how the buoyant lithosphere sinks into the dense asthenosphere. Davis and Darby (2010) and Wang et al. (2012) proposed that large-scale crustal stretch/extension occurred across the northeastern section of continental Asia in the late Cretaceous by studying the metamorphic core complexes. They further suggested that the post-orogenic collapse of the Okhotsk orogenic processes can be responsible for the weaker destruction of the west NCC. However, this model lacks a physically plausible mechanism to explain the lithosphere thinning and related volcanism.

It is now well understood that there are three basic mechanisms through which a solid rock can be partially melt to form magmas (see Niu, 2005): (1) heating, (2) decompression, and (3) volatile addition. As discussed above, heating is unlikely as the effective mechanism for the lithosphere thinning and magmatism in the NCC. Decompression melting can explain the petrogenesis of basaltic magmatism at ocean ridges and in rifting areas, but basalts in these settings differ from those in the NCC. While the traditional 'lithosphere delamination' is an interesting concept, it has physical difficulties in causing lithosphere thinning and thus related magmatism. Post-orogenic extension is a vague description without mechanism for large scale lithosphere thinning and related magmatism. Volatile addition, thus, deserves attention in causing lithosphere thinning and the petrogenesis of the 119.6–108.6 Ma basalts in the Jining area.

Niu (2005) suggested that the water released from the subducted oceanic lithosphere in the mantle transition zone beneath eastern China will rise in the form of hydrous melt through the upper asthenospheric mantle and reach the lithosphere. This hydrous melt can effectively hydrate the base of the existing lithosphere and convert its deep portion into asthenosphere in terms of physical properties such as viscosity. This is a physically straightforward mechanism to account for the lithosphere thinning in the east NCC (the region east to the GGL). Whether such mechanism works in the west NCC remains unknown because it is uncertain whether Paleo-Pacific slab indeed exited beneath the west NCC in the Mesozoic. Niu (2005) estimated that a period of ~75 Myrs is needed for Plaeo-Pacific slab to "reach" 110°E underneath the NCC since the subduction. On the other hand, the 138 Ma granite in Siziwang Qi (Nie et al., 2009) is interpreted as evidence that Plaeo-Pacific slab may have reached underneath the Jining area in the early Cretaceous.

It should be noted that the seismically-observed transition-zone slab beneath eastern China is linked to the present-day western Pacific subduction zone that is no older than ~60 Ma. However, there are many lines of evidence for the presence of the same or similar transition-zone slab back in the Mesozoic as indicated by the widespread Yanshannian granitoids throughout eastern China from NE to SE, which marks the presence of an active continental margins related to northwestward subduction of the Paleo-Pacific seafloor (Niu, 2014). Hence, the basal hydration-weakening (Niu, 2005) remains the physically most plausible mechanism to have caused the mantle lithosphere thinning beneath the NCC, including the western locations on various

local scales such as beneath the Jining area in the Mesozoic (to explain the 119.6–108.6 Ma basalt magmatism) although more work is needed to test this hypothesis. In this context, it should be noted that subducted Paleo-Asian Ocean slabs from the north is unlikely to have provided water for hydrating the lithospheric mantle beneath the NCC (Niu, 2014) because that slab had subducted into the lower mantle (>150 Ma, >2500 km; Van der Voo et al., 1999).

5.6.2. The geodynamics of the Cenozoic volcanism in the west NCC

The petrogenesis of Cenozoic basalts in the NCC has been in hot debate. Ren et al. (2002) and Tang et al. (2006) considered India–Eurasia continental collision as the major cause to induce the asthenosphere upwelling beneath the NCC. However, Zhao et al. (2011) showed no direct correlation of mantle flow beneath the NCC with the India–Eurasia collision based on the study of new SKS wave splitting measurements.

Niu (2005) offered a new hypothesis. In this hypothesis, western Pacific wedge suction draws asthenospheric material to flow from the west to beneath eastern China. The eastward asthenospheric flow from beneath eastern China, in turn, requires material replenishment further from the west again. Because the thickened lithosphere beneath the plateaus in western China contrasts the thinned lithosphere beneath the hilly plains in eastern China, the asthenospheric replenishment from beneath the plateaus to beneath eastern China must experience decompression. And this decompression can cause the flowing asthenosphere to melt and give rise to the Cenozoic volcanism in eastern China (see Niu, 2005). We consider this as a logically sound hypothesis, but further effort is needed to test this hypothesis. As the Jining Cenozoic volcanic province is the westernmost Cenozoic volcanic province located in the NCC, we consider that Jining area should be the first place to experience the decompression of eastward asthenospheric flow. Thus the Jining Cenozoic basalts (both of 23.5–21.9 Ma and 1.3–0.11 Ma) may be the very product from such a decompression melting.

5.6.3. A model for the lithosphere evolution

The foregoing discussion allows us to vision the lithosphere evolution schematically shown in Fig. 13. It illustrates the spatial and temporal variation of the lithosphere under the Jining volcanic province. As shown in Fig. 13a, the lithosphere in Jining area was thick and fertile before 119.6 Ma. The metasomatic veins were long before formed by accreting the subjacent volatile (H_2O, CO_2, etc.) and incompatible element enriched material (Niu, 2008; Niu and O'Hara, 2003). Fig. 13b illustrates that the water released from the transition-zone slabs and hydrous melt can hydrate and weaken the basal portion of the existing lithosphere, whose melting produced the Jining 119.6–108.6 Ma volcanism. The lithosphere under such area evolved, from the early Cretaceous to the Miocene, to become more depleted as the enriched components have been progressively melted and extracted; this process eventually transformed the lower portion of the ancient lithospheric mantle into the asthenospheric mantle in terms of physical properties. In the Cenozoic, the melt generated from partial melting of the metasomatized asthenosphere randomly assimilated the early formed metasomatized vein lithologies within the overlying lithosphere during ascent, producing the Jining 23.5–21.9 Ma basalts (Fig. 13c). Lithosphere thinning in the west NCC is a diachronous process and this thinning continues to the present. The Jining Quaternary basalts represent the products derived from asthenosphere beneath the thinned and thinner lithosphere than that during the 23.5–21.9 Ma magmatism as illustrated in Fig. 13d.

6. Conclusions

1. The Jining 119.6–108.6 Ma basalts resulted from partial melting of ancient metasomatized lithospheric mantle most likely caused by basal hydration of water (hydrous melt) released from the Paleo-Pacific slab in the mantle transition zone. We interpret this volcanism as indicating the lithosphere thinning in the west NCC.
2. The Jining Cenozoic basalts (both of 23.5–21.9 Ma and 1.3–0.11 Ma) resulted from decompression melting of eastward flowing asthenosphere. The 23.5–21.9 Ma incipient melt assimilated ancient metasomatized lithosphere during melt ascent, while the Jining 1.3–0.11 Ma basalts are produced as a result of continued decompression melting beneath the even thinner lithosphere.
3. The lithosphere under the west NCC has been thinning since the early Cretaceous and this thinning continues to the present.

Acknowledgment

We thank Piaoer Fu, Wenli Sun, and Yuxin Ma for their field company and samples preparing for the geochemistry analysis. We acknowledge Yueheng Yang, Chaofeng Li, Xianghui Li, Entao Liu and Wei Zhou for the assistance with Sr–Nd–Hf isotope separation; Huaikun Li, Hongying Zhou, Guozhan Li and Yurong Cui for Sr isotope detecting; and Prof. Lian Zhou and Jing Li for Nd isotope detecting. We thank two anonymous reviewers and the editor Andrew Kerr for their constructive reviews. This work was supported by the National Natural Science Foundation of China (NSFC grants 91014003 and 41130314).

Appendix 1. The averaged trace element (ppm) analyses results of the standards

Sample	AGV-2 N=6	GSR-1 N=3	GSR-3 N=3	Sample	AGV-2 N=6	GSR-1 N=3	GSR-3 N=3
Li	10.7	134	9.60	Ce	67.1	104	105
Sc	13.1	6.15	14.6	Pr	8.14	12.0	12.6
Ti	6397	1711	14065	Nd	28.9	45.6	48.8
V	117	23.4	171	Sm	5.23	9.36	10.2
Cr	17.2	3.73	138	Eu	1.55	0.77	3.04
Co	15.2	3.23	48.1	Gd	4.59	8.49	8.49
Ni	17.8	2.35	145	Tb	0.64	1.51	1.10
Cu	52.7	3.14	49.7	Dy	3.35	9.75	5.49
Zn	87.9	28.0	125	Ho	0.67	2.09	0.91
Ga	20.6	18.7	23.7	Er	1.75	6.12	1.87
Rb	66.6	454	38.8	Tm	0.26	1.04	0.26
Sr	637	108	1146	Yb	1.54	7.08	1.42
Y	18.8	66.9	23.1	Lu	0.25	1.07	0.18
Zr	239	159	281	Hf	5.22	6.39	6.61
Nb	15.4	41.5	72.0	Ta	0.92	7.18	4.42
Cs	1.13	36.5	0.68	Pb	12.4	30.1	8.02
Ba	1125	316	525	Th	5.90	50.2	5.78
La	37.7	50.3	54.5	U	1.73	18.4	1.41

N denotes the number of the standerands during our analysis.

Appendix 2. The Sr-Nd-Hf isotope replicate analyses results of the international reference materials

	$^{87}Sr/^{86}Sr$	±2σ	$^{143}/^{144}Nd$	±2σ	$^{176}Hf/^{177}Hf$	±2σ
BHVO-2[a]	0.703472	0.000003	0.512982	0.000003	0.283074	0.000027
BHVO-2[a]			0.512989	0.000003	0.283085	0.000021
BCR-2[a]	0.704990	0.000003	0.512624	0.000003	0.282868	0.000021
BCR-2[a]	0.705006	0.000003	0.512635	0.000004	0.282867	0.000022
BHVO-2[b]	0.703468	0.000012	0.512988	0.000005	0.283105	0.000007
BHVO-2[b]	0.703471	0.000011	0.512979	0.000006	0.283098	0.000008
BCR-2[b]	0.705003	0.000010	0.512633	0.000007	0.282854	0.000007
BCR-2[b]	0.705003	0.000010	0.512639	0.000005	0.282866	0.000005

a. Bulk-rock Sr, Nd and Hf elemental separation was done at Institute of Geology and Geophysics (Beijing), Chinese Academy of Sciences; Strontium isotope ratios were determined using Thermal Ionization Mass Spectrometer (TIMS) in Tianjin Institute of Geology and Mineral Resources; Neodymium isotope ratios were determined using Multi-Collector Inductively Coupled Plasma Mass Spectrometer (MC ICP-MS) at China University of Geosciences, Wuhan (CUGW); Hafnium isotopic ratios were determined using MC ICP-MS at Institute of Geology and Geophysics (Beijing), Chinese Academy of Sciences.
b. Bulk-rock Sr, Nd and Hf elemental separation and determination (using MC ICP-MS) were done in the Radiogenic Isotope Facility at the University of Queensland, Australia.

References

Bai, Z.D., Wang, J.M., Xu, G.L., Liu, L., Xu, D.B., 2008. Quaternary volcano cluster of Wulanhada, Right-Back-Banner, Chahaer, Inner Mongolia. Acta Petrologica Sinica 24, 2585–2594 (in Chinese with English abstract).

Basu, A.R., Wang, J.W., Huang, W.K., Xie, G.H., Tatsumoto, M., 1991. Major element, REE and Pb, Nd and Sr isotopic geochemistry of Cenozoic volcanic rocks of eastern China: implications for origin from suboceanic-type mantle reservoirs. Earth and Planetary Science Letters 105, 149–169.

Carlson, R.W., Pearson, D.G., James, D.E., 2005. Physical, chemical, and chronological characteristics of continental mantle. Reviews of Geophysics 43 (1).

Charlier, B., Namur, O., Duchesne, J.C., Wiszniewska, J., Parecki, A., Vander Auwera, J., 2009. Cumulate origin and polybaric crystallization of Fe–Ti oxide ores in the Suwalki anorthosite, northeastern Poland. Economic Geology 104, 205–221.

Chen, G.D., 1960. Theory of Activation of Platforms and its Significance in Ore Searching. Geological Press, Beijing pp. 1–408 (in Chinese with English abstract).

Chen, L., 2010. Concordant structural variations from the surface to the base of the upper mantle in the North China Craton and its tectonic implications. Lithos 120, 96–115.

Chen, Y., Wu, T.R., Xu, X., Zhang, S.T., 2004. Discovery of mantle xenoliths bearing Miocene potassium-rich olivine basalt and its significance in Siziwang Qi area, Inner Mongolia. Geological Journal of China Universities 10, 586–591 (in Chinese with English abstract).

Chen, L., Cheng, C., Wei, Z., 2009. Seismic evidence for significant lateral variations in lithospheric thickness beneath the central and western North China Craton. Earth and Planetary Science Letters 286, 171–183.

Davis, G.A., Darby, B.J., 2010. Early Cretaceous overprinting of the Mesozoic Daqing Shan fold-and-thrust belt by the Hohhot metamorphic core complex, Inner Mongolia, China. Geoscience Frontiers 1, 1–20.

Deng, J.F., 1988. Continental rift magmatism and deep process. In: Chi, J.S. (Ed.), Cenozoic Basalt and Upper Mantle of Eastern China. China University of Geosciences Press, Wuhan, pp. 201–218 (in Chinese).

Deng, J.F., Zhao, H.L., Luo, Z.H., Guo, Z.F., Mo, X.X., 1998. Mantle plumes and lithosphere motion in East Asia. In: Flower, M., Chung, S.L., Lo, C.H., Lee, T.Y. (Eds.), Mantle Dynamics and Plate Interactions in East Asia. American Geophysical Union, Washington D.C., pp. 59–65.

Deng, J.F., Mo, X.X., Zhao, H.L., Wu, Z.X., Luo, Z.H., Su, S.G., 2004. A new model for the dynamic evolution of Chinese lithosphere: 'continental roots–plume tectonics'. Earth Science Reviews 65, 223–275.

DePaolo, D.J., Daley, E.E., 2000. Neodymium isotopes in basalts of the southwest basin and range and lithospheric thinning during continental extension. Chemical Geology 169, 157–185.

Ellam, R.M., 1992. Lithospheric thickness as a control on basalt geochemistry. Geology 20, 153–156.

Fan, W.M., Zhang, H.F., Baker, J., Jarvis, K.E., Mason, P.R.D., Menzies, M.A., 2000. On and off the North China Craton: where is the Archaean keel? Journal of Petrology 41, 933–950.

Furman, T., 1995. Melting of metasomatized subcontinental lithosphere: undersaturated mafic lavas from Rungwe, Tanzania. Contributions to Mineralogy and Petrology 122, 97–115.

Gao, S., Luo, T.C., Zhang, B.R., Zhang, H.F., Han, Y.W., Zhao, Z.D., Hu, Y.K., 1998. Chemical composition of the continental crust as revealed by studies in East China. Geochimica et Cosmochimica Acta 62, 1959–1975.

Gao, S., Rudnick, R.L., Carlson, R.W., McDonough, W.F., Liu, Y.S., 2002. Re–Os evidence for replacement of ancient mantle lithosphere beneath the North China Craton. Earth and Planetary Science Letters 198, 307–322.

Gao, S., Rudnick, R.L., Yuan, H.L., Liu, X.M., Liu, Y.S., Xu, W.L., Ling, W.L., Ayers, J., Wang, X.C., Wang, Q.H., 2004. Recycling lower continental crust in the North China Craton. Nature 432, 892–897.

Gao, S., Zhang, J.F., Xu, W.L., Liu, Y.S., 2009. Delamination and destruction of the North China Craton. Chinese Science Bulletin 54, 3367–3378.

Griffin, W.L., Zhang, A.D., O'Reilly, S.Y., Ryan, C.G., 1998. Phanerozoic evolution of the lithosphere beneath the Sino-Korean Craton. In: Flower, M., Chung, S.L., Lo, C.H., Lee, T.Y. (Eds.), Mantle Dynamics and Plate Interactions in East Asia. American Geophysical Union, Washington D.C., pp. 107–126.

Guo, P.Y., Niu, Y.L., Yu, X.H., 2014. A synthesis and new perspective on the petrogenesis of kamafugites from West Qinling, China, in a global context. Journal of Asian Earth Sciences 79, 86–96.

Han, B.F., Wang, S.G., Kagami, H., 1999. Trace element and Nd–Sr isotope constraints on origin of the Chifeng flood basalts, North China. Chemical Geology 155, 187–199.

Hawkesworth, C.J., Erlank, A.J., Kempton, P.D., Waters, F.G., 1990. Mantle metasomatism: isotope and trace-element trends in xenoliths from Kimberley, South Africa. Chemical Geology 85, 19–34.

He, Y.K., Wu, T.R., Jing, X., Luo, H.L., Zhao, L., 2009. Early Cretaceous underplating of the north margin of North China Craton: evidences from the granulite xenoliths. Acta Petrologica Sinica 25, 1201–1215 (in Chinese with English abstract).

Ho, K.S., Liu, Y., Chen, J.C., Yang, H.J., 2008. Elemental and Sr–Nd–Pb isotopic compositions of late Cenozoic Abaga basalts, Inner Mongolia: implications for petrogenesis and mantle process. Geochemical Journal 42, 339–357.

Ho, K.S., Liu, Y., Chen, J.C., You, C.F., Yang, H.J., 2011. Geochemical characteristics of Cenozoic Jining basalts of the western North China Craton: evidence for the role of the lower crust, lithosphere, and asthenosphere in petrogenesis. Terrestrial, Atmospheric and Oceanic Sciences 22, 15–40.

Hofmann, A.W., Jochum, K.P., Seufert, M., White, W.M., 1986. Nb and Pb in oceanic basalts: new constraints on mantle evolution. Earth and Planetary Science Letters 79, 33–45.

Humphreys, E.R., Niu, Y.L., 2009. On the composition of ocean island basalts (OIB): the effects of lithospheric thickness variation and mantle metasomatism. Lithos 112, 118–136.

Jahn, B.M., Auvray, B., Comichet, J., Bai, Y.L., Shen, Q.H., Liu, D.Y., 1987. 3.5 Ga old amphibolites from eastern Hebei province, China: field occurrence, petrography, Sm–Nd isochron age and REE geochemistry. Precambrian Research 34, 311–346l.

Jing, X., Wu, T.R., He, Y.K., 2010. The geological environment of the xenolith-bearing Miocene basalt from Siziwang County, Inner Mongolia. Acta Scientiarum Naturalium Universitatis Pekinensis 46, 215–223 (in Chinese with English abstract).

Kárason, H., Van der Hilst, R.D., 2000. Constraints on mantle convection from seismic tomography. The History and Dynamics of Global Plate Motions, 121 pp. 277–288.

Kuritani, T., Ohtani, E., Kimura, J.I., 2011. Intensive hydration of the mantle transition zone beneath China caused by ancient slab stagnation. Nature Geoscience 4, 713–716.

A Classification of Igneous Rocks and Glossary of Terms. In: Le Maitre, R.W. (Ed.), Blackwell, Oxford, pp. 1–193.

Li, Y., Wu, T.R., Luo, H.L., Zhao, L., 2006. Geochemistry and tectonic setting of the early Cretaceous shoshonite of Siziwangqi area, Inner Mongolia. Acta Petrologica Sinica 22, 2791–2800 (in Chinese with English abstract).

Liu, D.Y., Nutman, A.P., Compston, W., Wu, J., She, Q., 1992. Remnants of >3800 Ma crust in the Chinese part of the Sino-Korean Craton. Geology 20, 339–342.

Liu, C.Q., Xie, G.H., Masuda, A., 1995a. Geochemistry of Cenozoic basalts from eastern China (I): major element and trace element compositions: petrogenesis and characteristics of mantle source. Geochemistry 24, 1–19 (in Chinese).

Liu, C.Q., Xie, G.H., Masuda, A., 1995b. Geochemistry of Cenozoic basalts from eastern China (II): Sr, Nd and Ce isotopic compositions. Geochemistry 24, 203–213 (in Chinese).

Liu, Y.S., Gao, S., Yuan, H.L., Zhou, L., Liu, X.M., Wang, X.C., Hu, Z.C., Wang, L.S., 2004. U–Pb zircon ages and Nd, Sr, and Pb isotopes of lower crustal xenoliths from North China Craton: insights on evolution of lower continental crust. Chemical Geology 211, 87–109.

Lloyd, F.E., Bailey, D., 1975. Light element metasomatism of the continental mantle: the evidence and the consequences. Physics and Chemistry of the Earth 9, 389–416.

Luo, X.Q., Chen, Q.T., 1990. Preliminary study on geochronology for Cenozoic basalts from Inner Mongolia. Acta Petrological et Mineralogica 9, 37–46 (in Chinese with English abstract).

Menzies, M.A., Xu, Y.G., 1998. Geodynamics of the North China Craton. In: Flower, M., Chung, S.L., Lo, C.H., Lee, T.Y. (Eds.), Mantle Dynamics and Plate Interactions in East Asia. American Geophysical Union, Washington D.C., pp. 155–165.

Menzies, M.A., Fan, W.M., Zhang, M., 1993. Palaeozoic and Cenozoic lithoprobes and the loss of >120 km of Archaean lithosphere, Sino-Korean Craton, China. Geological Society, London, Special Publications 76, 71–81.

Mikova, J., Denkova, P., 2007. Modified chromatographic separation scheme for Sr and Nd isotope analysis in geological silicate samples. Journal of Geosciences 52, 221–226.

Nie, F.J., Xu, D.Q., Jiang, S.H., Hu, P., 2009. Zircon SHRIMP U–Pb dating of K-feldspar granite samples from the Aobaotu granite stock in the Su-Cha (Sumoqagan Obo) fluorite ore district, Inner Mongolia. Acta Geoscientica Sinica 30, 803–811 (in Chinese with English abstract).

Niu, Y.L., 2005. Generation and evolution of basaltic magmas: some basic concepts and a hypothesis for the origin of the Mesozoic and Cenozoic volcanism in eastern China. Geological Journal of China University 11, 9–46.

Niu, Y.L., 2008. The origin of alkaline lavas. Science 320, 883–884.

Niu, Y.L., 2014. Subduction initiation, trench retreat and global tectonic consequences: the origin of backarc basins in the western Pacific and effect on eastern China geology since the Mesozoic. In: Zhai, M.G., Xiao, W.J. (Eds.), Plate Tectonics, Geological Events and Resources: New Advances in Geological Sciences. Science Press, Beijing (Pages 15 pp.).

Niu, Y.L., Batiza, R., 1997. Trace element evidence from seamounts for recycled oceanic crust in the eastern equatorial Pacific mantle. Earth and Planetary Science Letters 148, 471–484.

Niu, Y.L., O'Hara, M.J., 2003. Origin of ocean island basalts: a new perspective from petrology, geochemistry, and mineral physics considerations. Journal of Geophysical Research 108 (B4), 2209. http://dx.doi.org/10.1029/200 2JB002048 (ECV 5 — 1 — 19).

Niu, Y.L., O'Hara, M.J., 2009. MORB mantle hosts the missing Eu (Sr, Nb, Ta and Ti) in the continental crust: new perspectives on crustal growth, crust–mantle differentiation and chemical structure of oceanic upper mantle. Lithos 112, 1–17.

Niu, Y.L., Waggoner, G., Sinton, J.M., Mahoney, J.J., 1996. Mantle source heterogeneity and melting processes beneath seafloor spreading centers: the East Pacific Rise 18°–19°S. Journal of Geophysical Research 101, 27711–27733.

Niu, Y.L., Regelous, M., Wendt, J.I., Batiza, R., O'Hara, M.J., 2002a. Geochemistry of near-EPR seamounts: importance of source vs. process and the origin of enriched mantle component. Earth and Planetary Science Letters 199, 327–345.

Niu, Y.L., Gilmore, T., Mackie, S., Greig, A., Bach, W., 2002b. Mineral chemistry, whole-rock compositions, and petrogenesis of Leg 176 gabbros: data and discussion. Proceedings of the Ocean Drilling Program, Scientific Results., 176, pp. 1–60.

Niu, Y.L., Wilson, M., Hymphreys, E.R., O'Hara, M.J., 2011. The origin of intra-plate ocean island basalts (OIB): the lid effect and its geodynamic implications. Journal of Petrology 52, 1443–1468.

Niu, Y.L., Wilson, M., Hymphreys, E.R., O'Hara, M.J., 2012. A trace element perspective on the source of ocean island basalts (OIB) and fate of subducted ocean crust (SOC) and mantle lithosphere (SML). Episodes 35, 310–327.

Peng, Z.C., Zartman, R.E., Futa, E., Chen, D.G., 1986. Pb-, Sr- and Nd- isotopic systematics and chemical characteristics of Cenozoic basalts, eastern China. Chemical Geology 59, 3–33.

Pilet, S., Baker, M.B., Stolper, E.M., 2008. Metasomatized lithosphere and the origin of alkaline lavas. Science 320, 916–919.

Pilet, S., Ulmer, P., Villiger, S., 2010. Liquid line of descent of a basanitic liquid at 1.5 Gpa: constraints on the formation of metasomatic veins. Contributions to Mineralogy and Petrology 159, 621–643.

Plank, T., Langmuir, C.H., 1998. The chemical composition of subducting sediment and its consequences for the crust and mantle. Chemical Geology 145, 325–394.
Ren, J., Tamaki, K., Li, S.T., Zhang, J.X., 2002. Late Mesozoic and Cenozoic rifting and its dynamic setting in eastern China and adjacent areas. Tectonophysics 344, 175–205.
Robinson, J.A.C., Wood, B.J., 1998. The depth of the spinel to garnet transition at the peridotite solidus. Earth and Planetary Science Letters 164, 277–284.
Sakuyama, T., Tian, W., Kimura, J.I., Fukao, Y., Hirahara, Y., Takahashi, T., Senda, R., Chang, Q., Miyazaki, T., Obayashi, M., Kawabata, H., Tatsumi, Y., 2013. Melting of dehydrated oceanic crust from the stagnant slab and of the hydrated mantle transition zone: constraints from Cenozoic alkaline basalts in eastern China. Chemical Geology 359, 32–48.
Song, Y., Frey, F.A., Zhi, X.C., 1990. Isotopic characteristics of Hannuoba basalts, eastern China: implications for their petrogenesis and the composition of subcontinental mantle. Chemical Geology 85, 35–52.
Sun, S.S., McDonough, W.F., 1989. Chemical and isotopic systematics of ocean basalt: implications for mantle composition and processes. Geological Society Special Publication 42, 323–345.
Tang, Y.J., Zhang, H.F., Ying, J.F., 2006. Asthenosphere–lithospheric mantle interaction in an extensional regime: implication from the geochemistry of Cenozoic basalts from Taihang Mountains, North China Craton. Chemical Geology 233, 309–327.
Van der Voo, R., Spakman, W., Bijwaard, H., 1999. Mesozoic subducted slabs under Siberia. Nature 397, 246–249.
Vervoort, J.D., Blichert-Toft, J., 1999. Evolution of the depleted mantle: Hf isotope evidence from juvenile rocks through time. Geochimica et Cosmochimica Acta 63, 533–556.
Wang, T., Guo, L., Zheng, Y.D., Donskaya, T., Gladkochub, D., Zeng, L.S., Li, J.B., Wang, Y.B., Mazukabzov, A., 2012. Timing and processes of late Mesozoic mid-lower-crustal extension in continental NE Asia and implications for the tectonic setting of the destruction of the North China Craton: mainly constrained by zircon U–Pb ages from metamorphic core complexes. Lithos 154, 315–345.
Wilson, M., 1989. Igneous Petrogenesis. Harper Collins Academic, London p. 466.
Wong, W.H., 1929. The Mesozoic orogenic movement in Eastern China. Bulletin of the Geological Society of China 8, 33–44.
Wu, F.Y., Walker, R.J., Ren, X.W., Sun, D.Y., Zhou, X.H., 2003. Osmium isotopic constraints on the age of lithospheric mantle beneath northeastern China. Chemical Geology 196, 107–129.
Wu, F.Y., Yang, Y.H., Xie, L.W., Yang, J.H., Xu, P., 2006. Hf isotopic compositions of the standard zircons and baddeleyites used in U–Pb geochronology. Chemical Geology 234, 105–126.
Wu, F.Y., Xu, Y.G., Gao, S., Zheng, J.P., 2008. Controversial on studies of the lithospheric thinning and craton destruction of North China. Acta Petrologica Sinica 24, 1145–1174 (in Chinese with English abstract).
Xu, Y.G., 2001. Thermo-tectonic destruction of the Archaean lithospheric keel beneath eastern China: evidence, timing and mechanism. Physics and Chemistry of the Earth, Part A: Solid Earth and Geodesy 26, 747–757.
Xu, Y.G., Chung, S.L., Ma, J.L., Shi, L.B., 2004. Contrasting Cenozoic lithospheric evolution and architecture in the Western and Eastern Sino-Korean Craton: constraints from geochemistry of basalts and mantle xenoliths. Journal of Geology 112, 593–605.
Xu, Y.G., Ma, J.L., Frey, F.A., Feigenson, M.D., Liu, J.F., 2005. Role of lithosphere–asthenosphere interaction in the genesis of Quaternary alkali and tholeiitic basalts from Datong, western North China Craton. Chemical Geology 224, 247–271.
Xu, W.L., Wang, Q.H., Wang, D.Y., Guo, J.H., Pei, F.P., 2006. Mesozoic adakitic rocks from the Xuzhou–Suzhou area, eastern China: evidence for partial melting of delaminated lower continental crust. Journal of Asian Earth Sciences 27, 454–464.
Yang, Y.H., Zhang, H.F., Xie, L.W., Liu, Y., Qi, C.S., Tu, X.L., 2006. Petrogenesis of typical Mesozoic and Cenozoic volcanic rocks from the North China Craton: new evidence from Hf isotopic studies. Acta Petrologica Sinica 22, 1665–1671.
Yang, Z.F., Luo, Z.H., Zhang, H.F., Zhang, Y.M., Huang, F., Sun, C.G., Dai, J.G., 2009. Petrogenesis and geological implications of the Tianheyong Cenozoic basalts, Inner Mongolia, China. Earth Science Frontiers 16, 90–106.
Yang, Y.H., Zhang, H.F., Chu, Z.Y., Xie, L.W., Wu, F.Y., 2010. Combined chemical separation of Lu, Hf, Rb, Sr, Sm and Nd from a single rock digest and precise and accurate isotope determinations of Lu–Hf, Rb–Sr and Sm–Nd isotope systems using Multi-Collector ICP-MS and TIMS. International Journal of Mass Spectrometry 290, 120–126.
Ye, H., Zhang, B., Mao, F., 1987. The Cenozoic tectonic evolution of the Great North China: two types of rifting and crustal necking in the Great North China and their tectonic implications. Tectonophysics 133, 217–227.
Yin, A., Nie, S., 1996. A Phanerozoic palinspastic reconstruction of China and its neighboring regions. In: Yin, A., Harrison, T.M. (Eds.), Tectonic Evolution of Asia. Cambridge University Press, Cambridge, pp. 442–485.
Yoder, H.S., Tilley, C.E., 1962. Origin of basalt magmas: an experimental study of natural and synthetic rock system. Journal of Petrology 3, 346–532.
Zhang, W.H., Han, B.F., 2006. K–Ar chronology and geochemistry of Jining Cenozoic basalts, Inner Mongolia, and geodynamic implications. Acta Petrologica Sinica 22, 1597–1607 (in Chinese with English abstract).
Zhang, H.F., Sun, M., Zhou, X.H., Fan, W.M., Zhai, M.G., Yin, J.F., 2002. Mesozoic lithosphere destruction beneath the North China Craton: evidence from major-, trace-element and Sr–Nd–Pb isotope studies of Fangcheng basalts. Contributions to Mineralogy and Petrology 144, 241–254.
Zhang, H.F., Sun, M., Zhou, X.H., Zhou, M.F., Fan, W.M., Zheng, J.P., 2003. Secular evolution of the lithosphere beneath the eastern North China Craton: evidence from Mesozoic basalts and high-Mg andesites. Geochimica et Cosmochimica Acta 67, 4373–4387.
Zhang, S.T., Wu, T.R., Xu, X., Byamba, J., Amarjargal, A., Wang, S.Q., Li, Z.Q., 2005. The significance of discovery of early Cretaceous shoshonite in central Inner Mongolia. Geological Journal of China Universities 41, 212–218 (in Chinese with English abstract).
Zhang, H.F., Goldstein, S.L., Zhou, X.H., Sun, M., Zheng, J.P., Cai, Y., 2008. Evolution of subcontinental lithospheric mantle beneath eastern China: Re–Os isotopic evidence from mantle xenoliths in Paleozoic kimberlites and Mesozoic basalts. Contributions to Mineralogy and Petrology 155, 271–293.
Zhang, H.F., Sun, Y.L., Tang, Y.J., Xiao, Y., Zhang, W.H., Zhao, X.M., Menzies, M.A., 2012a. Melt–peridotite interaction in the Pre-Cambrian mantle beneath the western North China Craton: petrology, geochemistry and Sr, Nd and Re isotopes. Lithos 149, 100–114.
Zhang, W.H., Zhang, H.F., Fan, W.M., Han, B.F., Zhou, M.F., 2012b. The genesis of Cenozoic basalts from the Jining area, northern China: Sr–Nd–Pb–Hf isotope evidence. Journal of Asian Earth Sciences 61, 128–142.
Zhao, D.P., 2009. Multiscale seismic tomography and mantle dynamics. Gondwana Research 15, 297–323.
Zhao, G.C., Wilde, S.A., Cawood, P.A., Sun, M., 2001. Archean blocks and their boundaries in the North China Craton: lithological, geochemical, structural and P–T path constraints and tectonic evolution. Precambrian Research 107, 45–73.
Zhao, L., Zheng, T.Y., Lu, G., Ai, Y.S., 2011. No direct correlation of mantle flow beneath the North China Craton to the India–Eurasia collision: constraints from new SKS wave splitting measurements. Geophysical Journal International 187, 1027–1037.
Zhao, X.M., Zhang, H.F., Su, F., Hu, Z.C., Lo, C.H., Wang, Y., Yang, S.H., Guo, J.H., 2013. Phlogopite $^{40}Ar/^{39}Ar$ geochronology of mantle xenoliths from the North China Craton: constraints on the eruption ages of Cenozoic basalts. Gondwana Research 23, 208–219.
Zhi, X.C., Song, Y., Frey, F.A., Feng, J.L., Zhai, M.Z., 1990. Geochemistry of Hannuoba basalts, eastern China: constraints on the origin of continental alkalic and tholeiitic basalt. Chemical Geology 88, 1–33.
Zhu, Y.S., Hou, G.S., Yang, J.H., 2012. Sources and petrogenesis of the Cenozoic alkali basalts in Hebi, eastern North China Craton: geochemical and Sr–Nd–Hf isotopic evidence. Acta Petrologica Sinica 28, 4064–4076 (in Chinese with English abstract).